

Doctoral Dissertation (Censored)

博士論文（要約）

**Discovery and Application of Size-Selective Rim Binding
Modes of Cyclodextrins**

（シクロデキストリン口縁部によるサイズ選択的結合能の発見
とその応用）

A Dissertation Submitted for the Degree of Doctor of Philosophy

December 2020

令和2年12月 博士（理学）申請

Department of Chemistry, Graduate School of Science,
The University of Tokyo

東京大学大学院 理学系研究科 化学専攻

Hiroki Hanayama

花山 博紀

Abstract

α , β , and γ -Cyclodextrins (CDs) made of six to eight glucose units resembles a doughnut shape and are produced on a 10,000-ton scale worldwide for solubilization of molecules in food, pharmaceutical, and other applications. The solubilization ability of CDs has almost entirely been assigned to cavity inclusion of molecules. Here, a question remains if it is the only binding mechanism, because we often find guests larger than the cavity.

In this thesis, I developed new chemistry of binding of CDs by using electron microscopic analysis to investigate equilibrium system in water for the first time.

Chapter 1 describes the concept of molecular recognition especially in chemistry known as host-guest chemistry, analytical methods for host-guest interaction, and the problem contained in the present analytical methods. In addition, I introduced a potential of single-molecule atomic-resolution real-time electron microscopy (SMART-EM) technique, which has achieved single molecular dynamics, reaction, kinetics, and minor chemical species in inhomogeneous mixture, for investigation of equilibrium system in host-guest chemistry of CDs.

第二章に関する記述については、5年以内に雑誌等で刊行予定のため非公開.

Chapter 3 describes the solubilization and purification of NH aggregates using CDs. CDs worked as a surfactant for a pointed surface of the apexes of NHs via mainly rim binding. Size recognition in rim binding enables efficient and selective solubilization of NH aggregates and separation of NH aggregates from horn-less impurity. As a result, gram-scale purification of NH aggregates was achieved and followed by the synthesis of impurity-free amino-NH aggregates.

Chapter 4 summarizes this thesis and describes possible outcomes of rim binding mode of CDs and SMART-EM technique developed in the present study.

Acknowledgement

I am very grateful to my supervisor, Prof. Dr. Eiichi Nakamura, who guided me through the process of writing this thesis. His enthusiasm, motivation, and immense knowledge helped me in not only research but also in the decision for my futures.

This thesis would not be possible without the support of Dr. Koji Harano. I am very grateful for all the discussions, which were essential for understanding the experimental results, and for the guidance in the whole research process.

I also wish to express my acknowledgement to Dr. Takayuki Nakamuro for his advice and discussion both in research and life.

I also thank Dr. Rui Shang for their helpful advice, suggestions, and encouragements.

I appreciate the support of all members from the subgroup studying electron microscopy; Mr. Toshiki Shimizu, Mr. Ryosuke Sekine, Mr. Ko Kamei, Mr. Hikaru Uchida, Mr. Dongxin Liu, Mr. Issei Tomotsuka, Mr. Keishi Takeuchi, Mr. Masaya Sakakibara, and Mr. Takato Ogata. I also thank the support from former members; Dr. Junya Yamada, Dr. Satoshi Okada, Dr. Prince Ravat, Dr. Dominik Lungerich, Dr. Junfei Xing, Dr. Chao Liu, Dr. Sai Maddala, Dr. Yuki Itabashi, Dr. Luca Schweighauser, Ms. Satori Kowashi, and Mr. Takuya Tsubota. I am especially grateful for the support of Mr. Toshiki Shimizu and Mr. Ryosuke Sekine, who spent the whole research life in the same laboratory and the same subgroup together. They have given me a strong support for me to work in this laboratory.

I am indebted to all my laboratory colleagues who showed immense support and patience to me. I also thank Dr. Takao Kaneko, Ms. Akemi Maruyama, and Mr. Koshi Chiba, who have supported the research in this laboratory.

I would like to thank MERIT that gave me financial support and providing an opportunity to research in a global view through my Ph.D. study.

Finally, I would like to express sincere gratitude to Mr. Kozo Hanayama and Ms.

Motoko Hanayama for their daily help, advice, and encouragement and for their continuous love.

Table of Contents

Abstract	i
Acknowledgement	ii
Table of Contents	iv
Abbreviation	vi
General introduction	1
1.1. Host-guest chemistry or Molecular recognition.....	3
1.1.1. Molecular recognition in biological systems	3
1.1.2. Molecular recognition in chemistry	4
1.2. Cyclodextrin	5
1.2.1. Cavity binding of cyclodextrin.....	6
1.2.2. Determination and characterization of cavity binding mode	8
1.3. SMART-EM analysis	11
1.3.1. SMART-EM analysis of key chemical species from mixture in solution	14
1.3.2. Carbon nanohorn	17
1.4. This work.....	17
1.5. References	19
第 2 章 本章については、5 年以内に雑誌等で刊行予定のため、非公開	23
Solubilization and purification of carbon nanohorn aggregates by using cyclodextrins as a surfactant	25
3.1. Introduction	27
3.1.1. Purification of carbon nanohorn aggregates.....	27
3.1.2. Superhydrophobicity	28
3.1.3 Utilization of cyclodextrins as a shape-cognitive dispersant of NHa for purification of GB from mixture	30
3.2. Results and discussion.....	30
3.2.1 Dispersion of NHa with CDs	30
3.2.2 Analysis of dispersed NHa	33
3.2.3 Re-dispersion of CD/NHa in water	35
3.2.4 A large-scale purification of NH aggregates by using α -CD	37
3.2.5 Synthesis of GB-free amino-NHa	40
3.3 Summary	43

3.4 Experimental section	44
3.4.1 Materials.....	44
3.4.2 General	44
3.4.3 Evaluation of dispersity of NHa via complexation with saccharides.....	44
3.4.4 Evaluation of the stability of CD/NHa complexes.....	44
3.4.5 TG analysis.....	45
3.4.6 Purification of NHa by complexation/decomplexation of α -CD.....	45
3.4.7 Purification of NHa by centrifugation of EtOH dispersion.....	46
3.4.8 Preparation of amino-NHa from purified NHa	46
Summary and Perspective	49

Abbreviation

Ac	acetyl
AFM	atomic force microscopy (microscope)
aq	aqueous solution
CB	cavity binding
CD	cyclodextrin
CNT	carbon nanotube
DLS	dynamic light scattering
DMSO	dimethyl sulfoxide
eq	equivalent
EM	electron microscopy
fps	frame per second
GB	graphitic ball-shaped impurity
M	molar (mol/L)
MM	molecular mechanics
MOF	Metal-organic framework
mp	melting point
ms	millisecond
NH	(carbon) nanohorn
NHa	carbon nanohorn aggregate
NMR	nuclear magnetic resonance
nRB	narrow rim binding
oB	other binding
RB	rim binding
SEM	scanning electron microscopy (microscope)
SMART-EM	Single-molecule atomic-resolution real-time electron microscopy
STM	scanning tunneling microscopy
TEM	transmission electron microscopy (microscope)
TG-DTA	thermogravimetry-differential thermal analysis
UV	ultraviolet
vdW	van der Waals
Vis	visible
wRB	wide rim binding
XRD	X-ray diffraction

Chapter 1.

General introduction

1. General Introduction

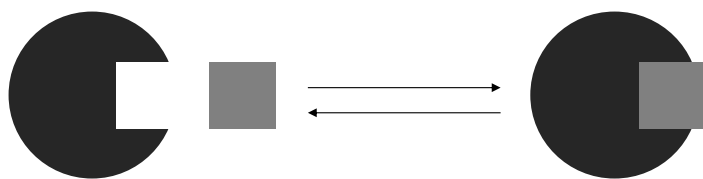
1.1. Host-guest chemistry or Molecular recognition

1.1.1. Molecular recognition in biological systems

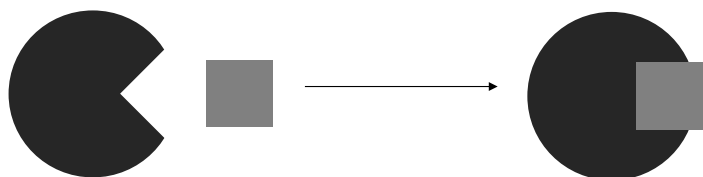
“Molecular recognition” is a specific interaction between two or more molecules driven by multiple non-covalent interactions, such as hydrogen bonding, van der Waals interaction, π - π interaction, and hydrophobic interaction.¹

Molecular recognition plays a crucial role in biological systems including the relationship between enzyme-ligand,² antigen-antibody,³ and sugar-lectin.⁴ The concept of molecular recognition was first proposed by Emil Fisher as a “Lock and key” hypothesis to explain the catalytic activity of enzymes with substrate molecules.⁵ In the hypothesis, an enzyme has a rigid active site to bind the guest strongly and shows a high catalytic activity (Figure 1-1a). There are some cases not completely explained from the “Lock and key” model,⁶ therefore the lock and key model was extended to the “induced-fit” model proposed by Daniel Koshland,⁷ where an active site is flexible and change its shape to achieve better fitting with a substrate molecule (Figure 1-1b). Recently, the “Conformational selection” model has been discussed as other mechanisms of molecular recognition in enzymes.⁸ This model also assumed conformational change of the active site; however, the change precedes the binding of molecules (Figure 1-1c). Thus, an enzyme takes various conformations including the conformation favorable for guest binding. At a time with the desired conformation, enzyme bound to substrate and equilibrium gradually shift toward the complex formation. These discussions showed the importance of dynamic equilibria of complicated molecules in the solution, and a new measurement technique is required to reveal dynamics of enzymes by direct investigation of each molecule.

(a) Lock and key model



(b) Induced-fit model



(c) Conformational selection model



Figure 1-1. Schematic illustration of binding between enzyme and substrate in (a) Lock and key model, (b) induced-fit model, and (c) conformational selection model.

1.1.2. Molecular recognition in chemistry

Inspired by the concept of molecular recognition especially in the “Lock and key” model, the chemistry of compounds that bind specific molecules has long been studied as host-guest chemistry.⁹ The host-guest chemistry was pioneered by Cramer since the 1940s for cyclodextrins (CDs, details are in the latter chapter),¹⁰ then the synthetic host molecules were investigated. One of the earliest synthetic molecules is crown ether (Figure 1-2). Crown ethers, which were synthesized by Charles Pederson in 1967,¹¹ were cyclic molecules that consist of several ether units. They size-selectively bind to certain cations by multiple coordination of lone pair of oxygen atoms to the cations.

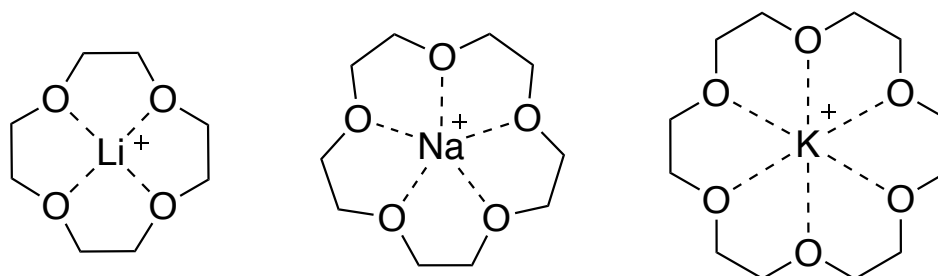


Figure 1-2. Representative molecular structure of crown ethers, which bind to alkali cations in size-selective way.

This finding paved the way in the host-guest chemistry, and various artificial host molecules were synthesized (Figure 1-3) to be applied to catalysis,¹² sensing,¹³ and drug delivery.¹⁴

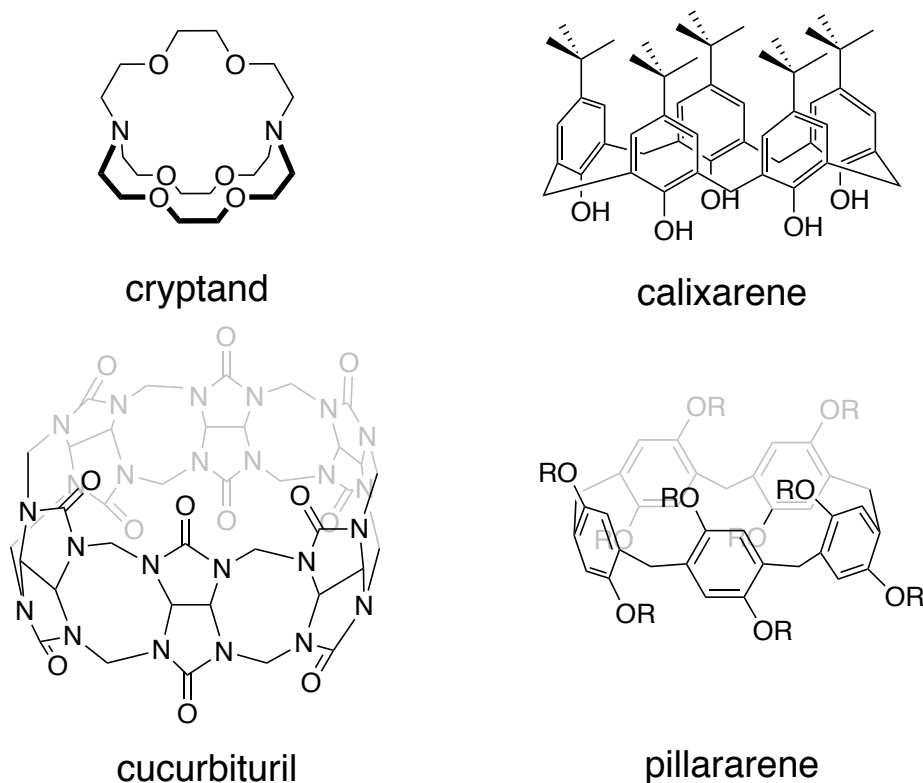


Figure 1-3. Molecular structures of representative synthetic host molecules.

1.2. Cyclodextrin

CDs are cyclic oligosaccharides made of six, seven, and eight α -D-glucose units (Figure 1-4), which was found by Antoine Villiers¹⁵ and proposed as a cyclic structure by Franz Schardinger.¹⁶ They possess a short tapered tubular structure with a hydrophobic cavity, a narrow rim made from primary hydroxy groups, and a wide rim composed of secondary hydroxy groups.

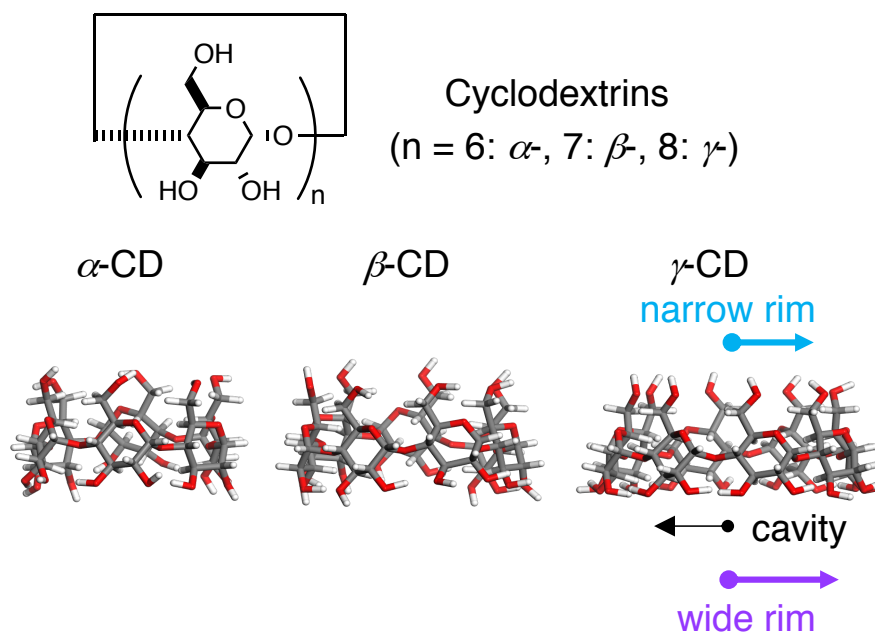


Figure 1-4. Crystal structures of cyclodextrins.

1.2.1. Cavity binding of cyclodextrin

CDs are another example of a compound that has been studied from the beginning in host-guest chemistry. They encapsulate hydrophobic molecules inside their cavity and solubilized in water. Combined with their availability due to mass production and non-toxicity, CDs continue to contribute to cutting-edge material science, while they have established industrial applications in food,¹⁷ pharmaceuticals,¹⁸ and many other fields. For example, an application for isolation and collection of gold from a mixture of various metals was reported.¹⁹ α -CD selectively formed one-dimensionally assembled 2:1 complex with gold salt and precipitated in water. In another example, Alsbaiee et al. reported the removal of organic pollutants in water by using polymerized β -CD.²⁰ The β -CD polymer (Figure 1-5a) efficiently removed both small aromatic compounds like 2-naphthol and relatively large bioactive compounds like ethinyl estradiol (Figure 1-5b). As shown in the latter example, CDs are characterized by their ability to bind a wide range of molecules, which is in clear contrast to the size-selective binding ability of crown ethers.

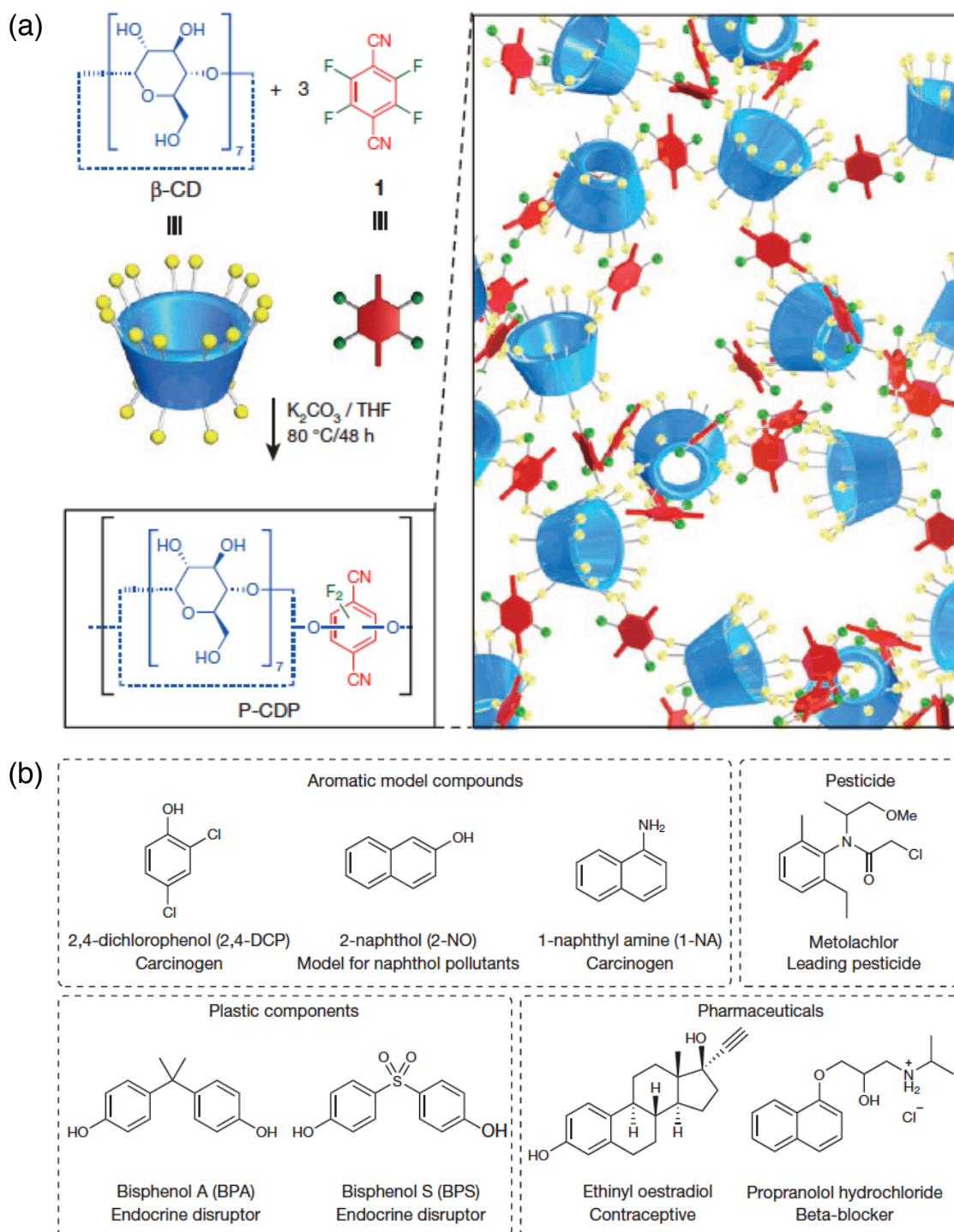


Figure 1-5. Removal of organic pollutants from water by β -CD-based polymer. (a) Preparation of β -CD-based polymer. (b) Molecular structure of organic pollutants, which were efficiently adsorbed by the polymer. Adapted with permission from ref. 20. Copyright 2016 Springer Nature.

1.2.2. Determination and characterization of cavity binding mode

In 1939, Freudenberg suggested that the cavity of CDs was hydrophobic and cyclodextrins could encapsulate molecules in their cavities, for the first time.²¹ Cramer and others continued to study complexation phenomena of CDs,¹⁰ however, cavity binding of cyclodextrin had not been confirmed until the end of the 1950s. In 1959, X-ray diffraction analysis showed that molecules like iodine could interact with the cavity of CDs,²² and the structure of inclusion complex was first confirmed for the complex between α -CD and potassium acetate using single crystal X-ray diffraction analysis in 1965.²³ After this report, crystal structures of inclusion complexes of cyclodextrins have been determined as evidence of cavity binding of CDs.

Based on the obtained crystal structures, almost all stoichiometric complexation between CD and molecule has been assigned as a cavity binding. Other than X-ray analysis, various spectroscopic analyses are applied to characterize complexes of CDs.

NMR spectroscopy is the simple and common method for characterization of inclusion complexes. CD has a six kind of hydrogens, and two of them (H_3 and H_5) are inside the cavity, while other four hydrogens are located outside of the cavity (Figure 1-6). H_3 is near the wide rim, and H_5 is near the narrow rim. When the inclusion complex is formed and guest molecule is encapsulated in the cavity, the NMR peaks of H_3 and H_5 show up-field shift as the average of the inclusion complex and free CD. The magnitude of shift depends on the structure of inclusion complex and the population of guest-bound and guest-free CD determined by the strength of the complexation. Therefore, a stoichiometry and binding strength of complexation cannot be determined from a single NMR measurement, and a series of NMR experiments with different molar ratio are required as described below.

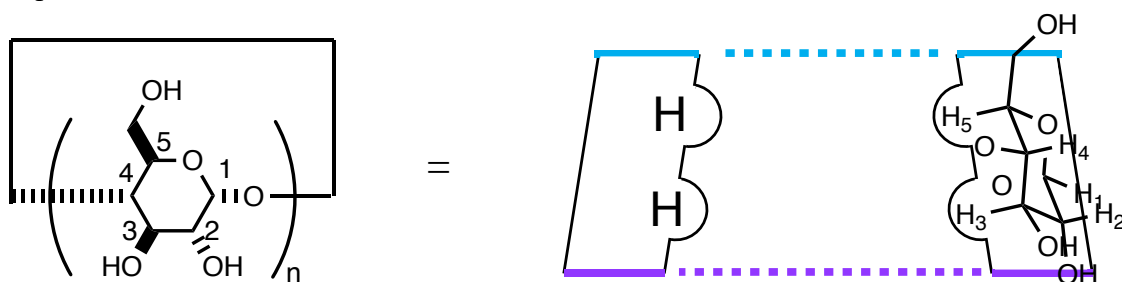


Figure 1-6. Schematic illustration of position of protons in cyclodextrins.

Job plot is an analytical technique used to determine the ratio of host and guest molecules in an inclusion complex.²⁴ In this method, the molar ratio of host and guest molecules is changed under the same total concentration. The chemical shift multiplied

by the fraction of the complex is plotted against the molar ratio. The molar ratio at the maximum of the plot corresponds to stoichiometry in the complex formation. However, there is a concern about the reliability of Job plot analysis, especially for a weakly binding system. Hibbert *et al.* demonstrated that simulated Job plots of a host-guest complex with 1:2 stoichiometry had a peak larger than 0.40 and difficult to assign as a 1:2 complex at 0.01 M (Figure 1-7).²⁵

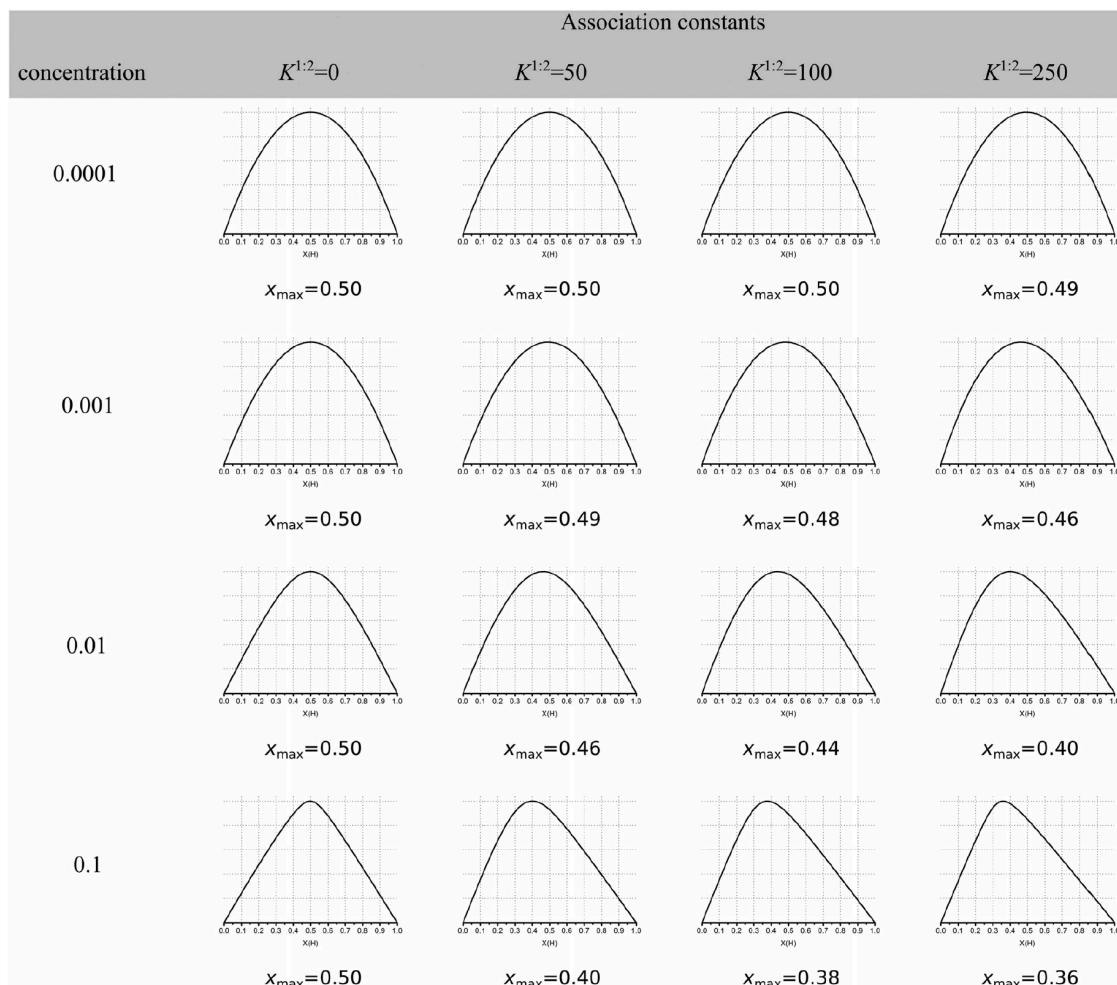


Figure 1-7. Simulation of Job plots for various associate constants and concentration. $K^{1:2}$ showed the ratio between 1:1 and 1:2 complex. In all cases, $K_I = 1000 \text{ M}^{-1}$. The obtained maximum point is shown as x_{\max} . Adapted with permission from ref. 25. Copyright 2016 Royal Society of Chemistry.

UV-vis spectroscopy can also be applied for the characterization of a complexation of cyclodextrins. CDs are not observed in UV-vis spectra, however, the absorption of the guest molecule is shifted by complexation. As same as NMR analysis, stoichiometry, a binding constant can be analyzed.

Other than spectroscopic analysis, thermogravimetric analysis (TGA) is sometimes utilized to determine the composition of an inclusion complex.²⁶ Moreover, the delay in the decomposition of the guest molecule is observed in the complexation.²⁷ Phase solubility study is a simple method to determine stoichiometry in the complex from the solubility change of hydrophobic guest molecule.²⁸ The increase of the concentration of the guest molecule is plotted against the concentration of added CD. The slope shows stoichiometry in the complexation, and the obtained diagram sometimes shows a non-linear relationship due to the presence of higher-order complexation (A_P , Figure 1-8) or formation of insoluble inclusion complexes (B_S , B_i).²⁹

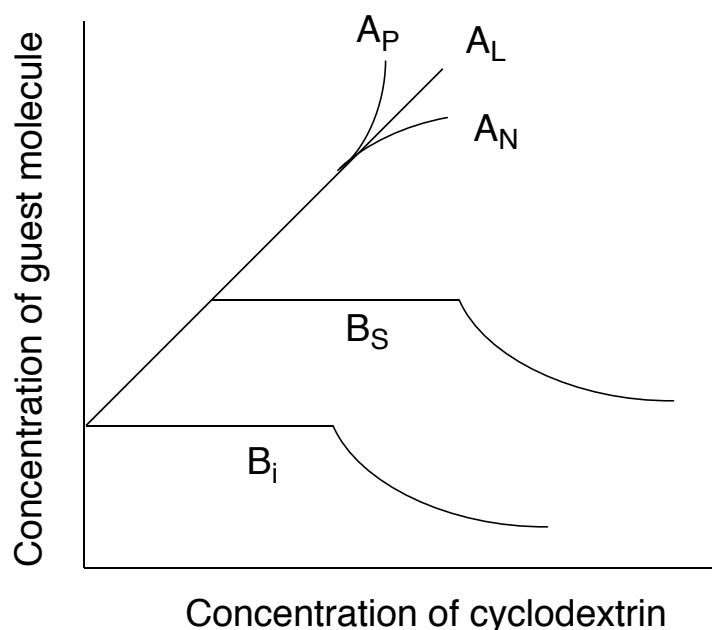


Figure 1-8. Phase-solubility diagram of CDs.

For the determination of complexation thermodynamics of CDs, NMR or UV measurements at different temperatures can be applied. Another important method is isothermal titration calorimetry, in which the exothermic or endothermic value during complexation was quantified to determine the binding constant, the stoichiometry, and the enthalpy change (ΔH) of complexation.³⁰ However, the application to the relatively weak complexation with binding constants about 10^3 M^{-1} is sometimes difficult and requires the determination of stoichiometry by another method.³¹

As I already mentioned in this chapter, there is a difficulty in the analysis of CD binding with multiple binding modes because it is impossible to analyze each chemical species in the equilibrium system from the previous methods. The spectroscopic and calorimetric analyses only provide information as an average of the entire equilibrium

system, which may miss minor species. Moreover, the spectral data does not allow us to determine the structure of the observed species. On the other hand, X-ray crystallography can only determine one isolated structure in the crystal, therefore the new analysis method to investigate each binding event structurally is required.

1.3. SMART-EM analysis

Structural analysis of organic compounds is the foundation of organic chemistry. Most of the discoveries in organic chemistry could not be achieved without structural analysis. Now, spectroscopic methods and X-ray crystallography are mainly used for structural analysis.^{32,33} In addition, observation of a single molecule by transmission electron microscopy (TEM) developed as a method for elucidation of time-resolved structural information³⁴ of a single organic molecule. This kind of information was not obtained from the conventional methods because they give us statistically averaged information about molecular structures. Single-molecular studies are often carried out using scanning tunneling microscopy (STM)^{35, 36} and atomic force microscopy (AFM).^{37,38,39} However, these scanning probe microscopies often lack time resolution and are difficult to apply to three dimensional molecules.

In 2007, Nakamura *et al.* reported the first time-resolved TEM observation of organic molecules, didocosanylcarborane.⁴⁰ The molecules were encapsulated in a single-wall carbon nanotube (CNT) to be fixed and to be isolated as single molecules. The motion of the alkyl chains in CNT was observed in second-order time resolution (Figure 1-9a).

They also succeeded in the observation of fullerenes or their derivatives in CNT and successfully visualized conformational change of the alkyl chain and the perfluoroalkyl chain of fullerene derivatives.⁴¹ Moreover, they reported a motion that the alkyl chain was squeezed out and pushed back through a hole defect of CNT (Figure 1-9b)⁴² and reactions between fullerenes (Figure 1-9c)⁴³. Importantly, a kinetic study of the reaction of fullerenes was achieved.⁴⁴ This result showed that statistical analysis of random single reaction events gave the value that described ensemble behavior of molecules, and suggested the possibility of kinetic and thermodynamic analysis by using TEM analysis.

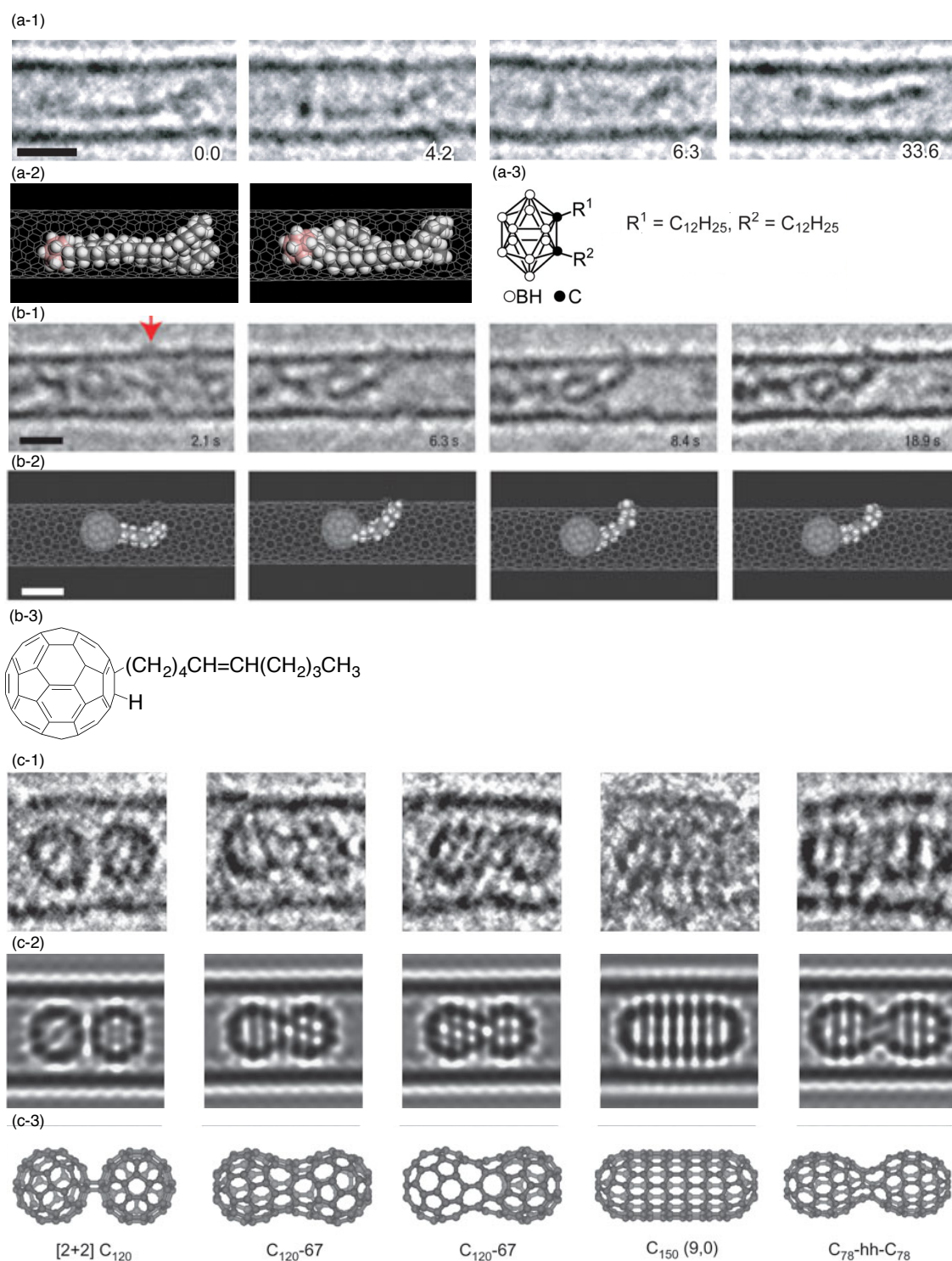


Figure 1-9. SMART-EM imaging of fullerene and organic molecules. (a) TEM imaging of didocosanylcarborane. (b) TEM imaging of the motion of alkenyl fullerene through a defect of CNT. (c) TEM observation of fullerene dimerization: (a,b,c-1) TEM images, (a,b,c-2) Simulation images, and (a,b,c-3) Simulation models. (Scale bar: 1nm in all the images) Adapted with permission from ref. 40 (a), 42 (b), and 43 (c). Copyright

2007 American Association for the Advancement of Science (a), 2008 Springer Nature (b), 2010 Springer Nature (c).

Since the encapsulation into CNT has a limitation in the size of target molecules, a fixation method of specimen molecule on an exterior of CNT has been developed by using carbon nanohorn aggregates (NH aggregates, discussed in a detail later) as a similar alternative. Amination of NH aggregates was achieved by mixing with NaNH_2 in liq. NH_3 as a solution and obtained amino groups mainly on the tip of NH were utilized to anchor a single molecule by covalent bonding.⁴⁵ First use of amino-NH was reported in 2008 to demonstrate TEM observation of the structure and conformational change of biotinylated triamide molecule fixed on NH (Figure 1-10).⁴⁶

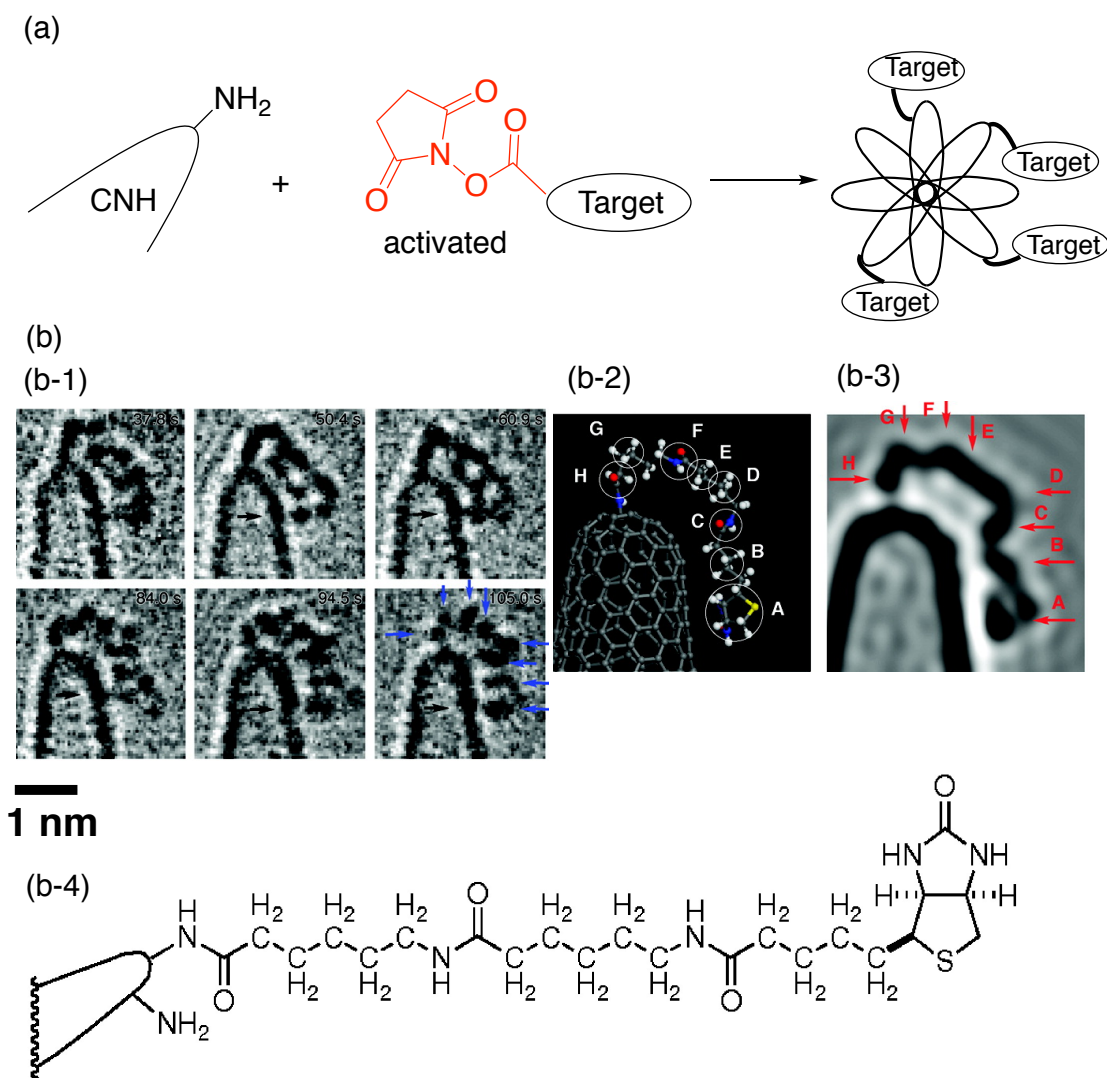


Figure 1-10. TEM observation of organic molecules on NHs. (a) Schematic illustration of target molecules binding to amino NH. (b) TEM observation of biotinylated triamide:

(b-1) A TEM image, (b-2) Simulation model, (b-3) Simulation image, and (b-4) The structure of observed compounds. Adapted with permission from ref. 46. Copyright 2008 American Chemical Society.

1.3.1. SMART-EM analysis of key chemical species from mixture in solution

SMART-EM analysis was applied for capturing intermediate structures in a solution enabled by the “fishhook” method. In the “fishhook” method, NH is modified with a certain functional group that can interact with a target, and the target structure attached to the NH is taken out from the solution to be analyzed by TEM. This method enables us to investigate the chemical species, which are hardly characterized other than single molecular level analysis because of low abundance ratio, inhomogeneous structure, and so on.

In 2012, a prenucleation cluster of an organic crystal was observed by using a fishhook method.⁴⁷ The intermediate of the crystal growth of 1,3,5-Tris(4-bromophenyl)benzene (Y molecule) was picked up with Y molecule covalently attached on NH (Figure 1-11a). SMART-EM analysis revealed that Y molecules were self-assembled into small clusters with disordered structure via π - π interaction in the early stage of crystal formation (Figure 1-11b, c, d), and the crystal growth proceeded on the two-step mechanism.

SMART-EM analysis also achieved the imaging of reaction intermediates in metal-organic framework (MOF) formation.⁴⁸ By using terephthalic acid as a fishhook, the intermediate structure in the synthesis of MOF-2 and -5 were investigated (Figure 1-12a). MOF-2 of two-dimensional structure and MOF-5 of three-dimensional structure were synthesized from zinc and terephthalic acid with different reaction temperatures. TEM observation showed that prenucleation clusters of each MOF already had a two- or three-dimensional structure corresponding to the finally obtained structure (Figure 1-12b, c). The result suggested that MOF-2 and -5 structures were determined at the prenucleation stage.

Two introduced studies succeeded to isolate and analyze the molecular assembly in the dynamic equilibrium in the solution and shows the possibility of grasping the entire complex equilibrium in a solution by statistical SMART-EM analysis.

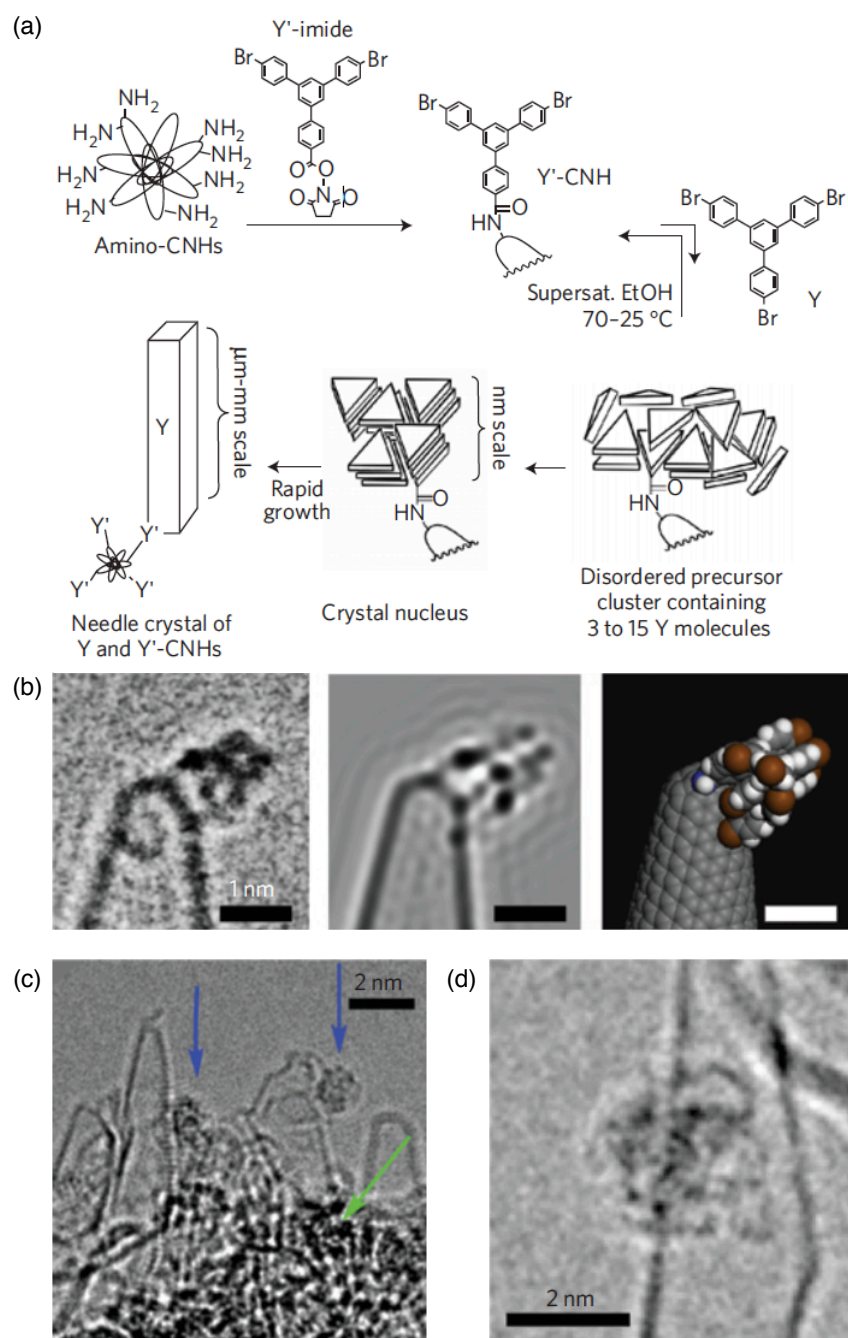


Figure 1-11. SMART-EM analysis of crystal nucleation. (a) Schematic image of crystal nucleation and growth of Y molecule on NH. (b) TEM image (left), its simulation (middle), and its molecular model of observed prenucleation cluster made from 3 Y molecule. (c) TEM image of two clusters (indicated by blue arrow) and a large aggregate on the surface of NH (indicated by a green arrow). (d) TEM image of disordered structure of assembly of 15 Y molecules. Adapted with permission from ref. 47. Copyright 2012 Springer Nature.

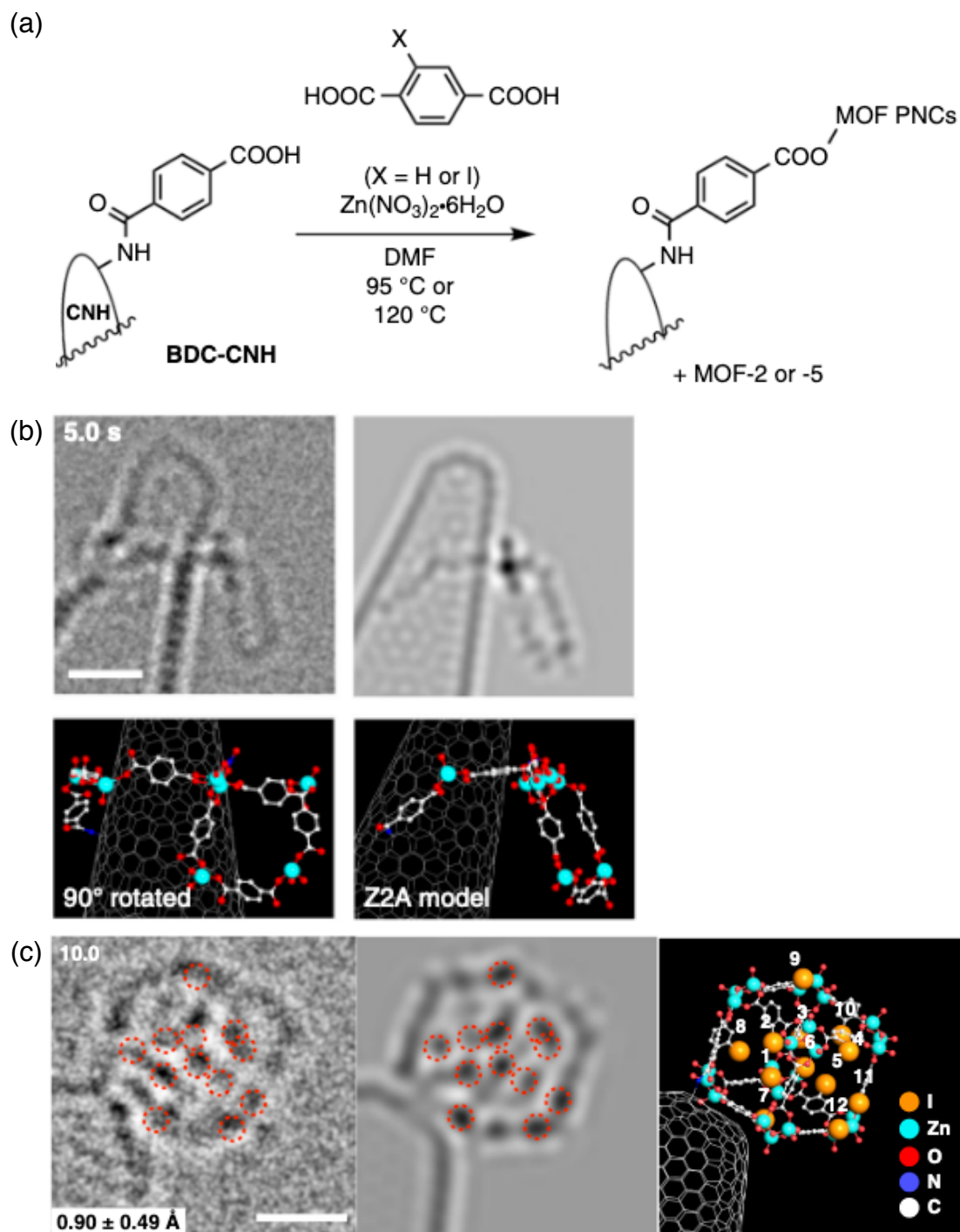


Figure 1-12. SMART-EM analysis of prenucleation cluster (PNC) in MOF-2 and -5 synthesis. (a) Fishhook method to capture MOF-2 and -5 intermediate. (b) TEM image, simulation, and model of two-dimensional PNC of MOF-2. (c) TEM image, simulation, and model of three-dimensional PNC of MOF-5. Adapted permission from ref. 48. Copyright 2019 Springer Nature.

1.3.2. Carbon nanohorn

NH aggregate is one of the nanocarbon materials, in which conical single-wall carbon nanotubes aggregate each other into 50–150 nm sized particles with their tips outside.⁴⁹ NH aggregates are synthesized by adding large energy such as arc discharge⁵⁰ or CO₂ laser⁵¹ to a carbon source. Vaporized carbon constructs NH structure by rapid cooling in inert gas. The synthesis of NH does not require a metal catalyst, and therefore the size of each NH is not controlled and inhomogeneous as observed in Figure 1-13.

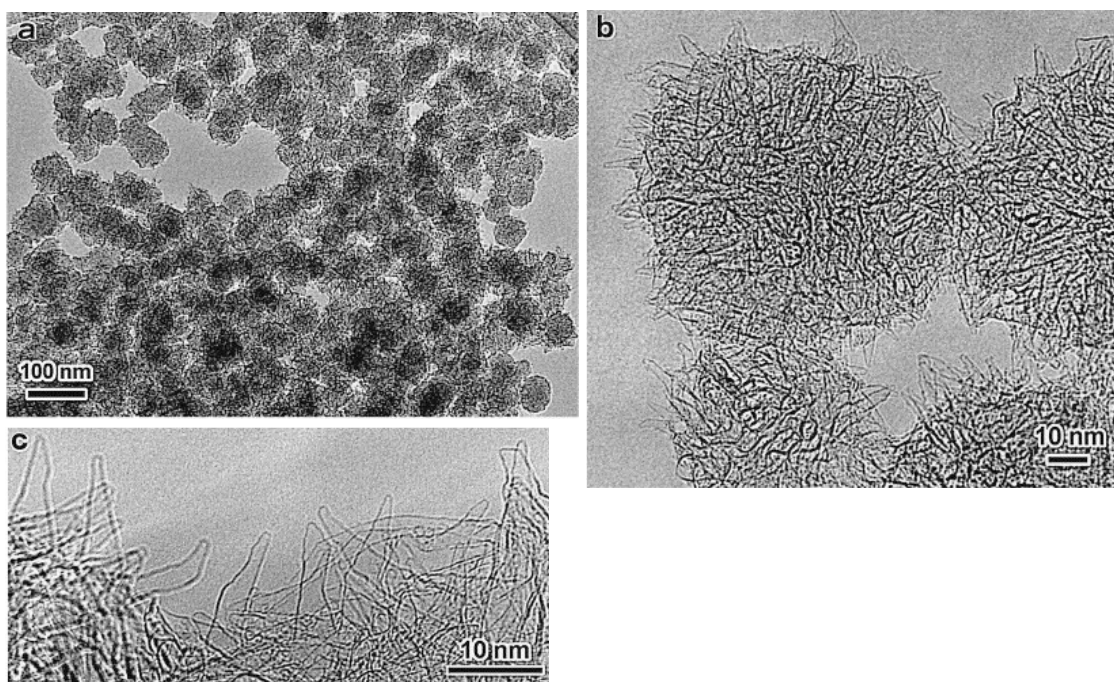


Figure 1-13. TEM images of NH aggregates (a) at a low magnification, (b) at a middle magnification, and (c) at a high magnification. Adapted with permission from ref. 51. Copyright 1999 Elsevier.

1.4. This work

As I introduced, cyclodextrins are utilized for solubilization of vast molecules in industrial and academic applications. However, a question remains if it is the only mechanism for all the applications where we find guest entities often larger than the cavity. A multitude of experiments have provided evidence that the binding of a guest hydrophobic molecule in the CD cavity entails the recognition, but little experimental evidence about other binding modes because of the lack of a method to detect other binding modes that may exist in the mobile binding equilibrium in water.

To probe the possibility of other binding modes in equilibrium, I conceived

SMART-EM analysis of CD binding on NH aggregates. Hemispherical apexes of NH aggregates acted as a solid-state library of hydrophobic molecules with different sizes widely and almost continuously distributed from smaller to larger sizes than the cavity of CD, and single molecular study enabled combinatorial analysis of binding of CDs to each NHs. I describe structural evidence for a doughnut-shaped molecule sitting on a hemisphere by the narrow or the wide rim in Chapter 2. Moreover, thermodynamic characterization was achieved by statistical analysis of observed TEM images. The thermodynamic parameters of the cavity and rim binding with those previously ascribed solely to cavity binding showed similar values and suggest that the rim binding occurs widely but has not been detected experimentally.

The rim binding of CDs to NHs was applied for solubilization and purification of NH aggregates from horn-less impurities as shown in Chapter 3. CDs bound to the tip of NH efficiently via rim binding and dispersed NH aggregates with only 1wt%, while glucose and amylose did not disperse NH aggregates with the same amount.

1.5. References

- 1 Breiten, B.; Lockett, M. R.; Sherman, W.; Fujita, S.; Al-Sayah, M.; Lange, H.; Bowers, C. M.; Heroux, A.; Krilov, G.; Whitesides, G. M. *J. Am. Chem. Soc.* **2013**, *135*, 15579–15584.
- 2 Ringe, D.; Petsko, G. A. *Science* **2008**, *320*, 1428–1429.
- 3 Sundberg, E. J.; Mariuzza, R. A. *Advances in Protein Chemistry* **2002**, *61*, 119–160.
- 4 Ambrosi, M.; Cameron, N. R.; Davis, B. G. *Org. Biomol. Chem.* **2005**, *3*, 1593–1608.
- 5 Fischer, E. *Chemischen Gesellschaft zu Berlin* **1894**, *27*, 2985–2993.
- 6 Thoma, J. A.; Koshland, D. E. *J. Am. Chem. Soc.* **1960**, *82*, 3329.
- 7 Koshland, D. E. *Proc. Natl. Acad. Sci. USA* **1958**, *44*, 98–104.
- 8 Savir, Y.; Tlusty, T.; *PLoS ONE* **2007**, *2*, e468.
- 9 Cram, D. J.; Cram, J. M. *Science* **1974**, *183*, 803–809.
- 10 Cramer, F.; Steinle, D. *Ann. Chem. Justus Liebigs* **1955**, *595*, 81.
- 11 Pedersen, C. J. *J. Am. Chem. Soc.* **1967**, *89*, 7017–7036.
- 12 Yoshizawa, M.; Tamura, M.; Fujita, M. *Science* **2006**, *312*, 251–254.
- 13 Gawley, R. E.; Pinet, S.; Cardona, C. M.; Datta, P. K.; Ren, T.; Guida, W. C.; Nydick, J.; Leblanc, R. M. *J. Am. Chem. Soc.* **2002**, *124*, 13448–13453.
- 14 Ma, D.; Hettiarachchi, G.; Nguyen, D.; Zhang, B.; Wittenberg, J. B.; Zavalij, P. Y.; Briken, V.; Isaacs, L. *Nat. Chem.* **2012**, *4*, 503–510.
- 15 Villiers, A. *Bull. Soc. Chim. Paris* **1891**, *45*, 468.
- 16 Schardinger, F. *Zentralbl. Bakteriolog., Parasitenkd., Infektionskrankh. Hyg., Abt 2* **1911**, *29*, 188.
- 17 Fenyvesi, É.; Vikmon, M.; Szenté, L. *Rev. Food Sci. Nutr.* **2016**, *56*, 1981–2004.
- 18 Loftsson, T.; Duchêne, D. *Int. J. Pharm.* **2007**, *329*, 1–11.
- 19 Liu, Z.; Frascioni, M.; Lei, J.; Brown, Z. J.; Zhu, Z.; Cao, D.; Iehl, J.; Liu, G.; Fahrenbach, A. C.; Botros, Y. Y.; Farha, O. K.; Hupp, J. T.; Mirkin, C. A.; Stoddart, J. F. *Nat. Commun.* **2013**, *4*, 1855.
- 20 Alsbaiee, A.; Smith, B. J.; Xiao, L.; Ling, Y.; Helbling, D. E.; Dichtel, W. R. *Nature* **2016**, *529*, 190–194.
- 21 Freudenberg, K. *Annu. Rev. Biochem.* **1939**, *8*, 81.
- 22 James, W. J.; French, D.; Rundle, R. E. *Acta Crystallogr.* **1959**, *12*, 385.
- 23 Hybl, A.; Rundle, R. E.; Williams, D. E. *J. Am. Chem. Soc.* **1965**, *87*, 2779.
- 24 Job, P. *Annales de Chimie* **1928**, *9*, 113–203.
- 25 Hibbert, D. B.; Thordarson, P. *Chem. Commun.* **2016**, *52*, 12792–12804.
- 26 Bai, Y.; Wang, J.; Bashari, M.; Hu, X.; Feng, T.; Xu, X.; Jin, Z.; Tian, Y. *Thermochim. Acta* **2012**, *541*, 62–69.

- 27 Ai, L.; Hu, J.; Ji, X. *RSC Advances* **2019**, 9, 26224–26229.
- 28 Higuchi, T.; Connors, K. A. *Adv. Anal. Chem. Instrum.* **1965**, 4, 117–212.
- 29 Loftsson, T.; Hreinsdóttir, D.; Másson, M. *Int. J. Pharm.* **2005**, 302, 18–28.
- 30 Rekharsky, M. V.; Inoue, Y. *Chem. Rev.* **1998**, 98, 1875–1917.
- 31 Turnbull, W. B.; Daranas, A. H. *J. Am. Chem. Soc.* **2003**, 125, 14859.
- 32 Palczewski, K.; Kumasaka, T.; Hori, T.; Behnke, C. A.; Motoshima, H.; Fox, B. A.; Le Trong, I.; Teller, D. C.; Okada, T.; Stenkamp, R. E.; Yamamoto, M.; Miyano, M. *Science* **2000**, 289, 739–745.
- 33 Fujita, D.; Yokoyama, H.; Ueda, Y.; Sato, S.; Fujita, M. *Angew. Chem. Int. Ed.* **2014**, 54, 155–158.
- 34 Nakamura, E. *Angew. Chem. Int. Ed.* **2012**, 52, 236–252.
- 35 Henzl, J.; Mehlhorn, M.; Gawronski, H.; Rieder, K.-H.; Morgenstern, K. *Angew. Chem. Int. Ed.* **2006**, 45, 603–606.
- 36 Mielke, J.; Hanke, F.; Peters, M. V.; Hecht, S.; Persson, M.; Grill, L. *J. Am. Chem. Soc.* **2015**, 137, 1844–1849.
- 37 Schuler, B.; Meyer, G.; Peña, D.; Mullins, O. C.; Gross, L. *J. Am. Chem. Soc.* **2015**, 137, 9870–9876.
- 38 Lassagne, B.; Tarakanov, Y.; Kinaret, J.; Garcia-Sanchez, D.; Bachtold, A. *Science* **2009**, 325, 1107–1110.
- 39 Schuler, B.; Fatayer, S.; Mohn, F.; Moll, N.; Pavlíček, N.; Meyer, G.; Peña, D.; Gross, L. *Nat. Chem.* **2016**, 8, 220–224.
- 40 Koshino, M.; Tanaka, T.; Solin, N.; Suenaga, K.; Isobe, H.; Nakamura, E. *Science* **2007**, 316, 853–853.
- 41 Harano, K.; Takenaga, S.; Okada, S.; Niimi, Y.; Yoshikai, N.; Isobe, H.; Suenaga, K.; Kataura, H.; Koshino, M.; Nakamura, E. *J. Am. Chem. Soc.* **2014**, 136, 466–473.
- 42 M. Koshino, N. Solin, T. Tanaka, H. Isobe, E. Nakamura, *Nat. Nanotechnol.* **2008**, 3, 595–597.^[1]
- 43 Koshino, M.; Niimi, Y.; Nakamura, E.; Kataura, H. *Nat. Chem.* **2010**, 2, 117–124.
- 44 Okada, S.; Kowashi, S.; Schweighauser, L.; Yamanouchi, K.; Nakamura, E. *J. Am. Chem. Soc.* **2017**, 139, 18281–18287.
- 45 Isobe, H.; Tanaka, T.; Maeda, R.; Noiri, E.; Solin, N.; Yudasaka, M.; Iijima, S.; Nakamura, E. *Angew. Chem. Int. Ed.* **2006**, 45, 6676–6680.
- 46 Nakamura, E.; Koshino, M.; Tanaka, T.; Niimi, Y.; Harano, K.; Nakamura, Y.; Isobe, H. *J. Am. Chem. Soc.* **2008**, 130, 7808–7809.
- 47 Harano, K.; Homma, T.; Niimi, Y.; Koshino, M.; Suenaga, K.; Leibler, L.; Nakamura, E. *Nat. Mater.* **2012**, 11, 877–881.

- 48 Xing, J.; Schweighauser, L.; Okada, S.; Harano, K.; Nakamura, E. *Nat. Commun.* **2019**, *10*, 3608.
- 49 Karousis, N.; Suarez-Martinez, I.; Ewels, C. P.; Tagmatarchis, N.; *Chem. Rev.* **2016**, *116*, 4850–4883.
- 50 Yamaguchi, T.; Bandow, S.; Iijima, S. *Chem. Phys. Lett.* **2004**, *389*, 181–185.
- 51 Iijima, S.; Yudasaka, M.; Yamada, R.; Bandow, S.; Suenaga, K.; Kokai, F.; Takahashi, K. *Chem. Phys. Lett.* **1999**, *309*, 165–170.

Chapter 2.

第 2 章 本章については，5 年以内に雑誌等で刊行予定のため，非公開

Chapter 3.

**Solubilization and purification of carbon nanohorn
aggregates by using cyclodextrins as a surfacetant**

3.1. Introduction

3.1.1. Purification of carbon nanohorn aggregates

Carbon nanohorn aggregates (NHa) are spherical aggregates of tapered shape carbon nanotubes with their tips exposed to the outside.¹ Due to the high surface area derived from its unique structure, NHa has potential for excellent gas adsorbant.² Moreover, NHa has also been studied in the area of biological application, such as a carrier in a drug delivery system³ and a target of photothermal cancer treatment.⁴ NHa is considered as a material with lower toxicity than carbon nanotube,⁵ because NHa does not require metal catalysts in its preparation.

NHa is prepared by CO₂ laser ablation on a graphite target.¹ However, 10% of sub-micrometer sized polygonal graphite particle, so-called graphitic ball-shaped impurity (GB, Figure 3-1a) formed together with NHa.⁶ Thermogravimetric analysis (TGA) showed GB burned at the higher temperature due to strong sp² bond in graphitic structure (Figure 3-1b). The purification of NHa is expected to enhance its function. The first purification of NH was reported by Bando et al.,⁷ however, they did not assess the purity quantitatively and the separation yield is under 40%. Zhang et al. reported separation of NHa and GBs with sodium dodecylbenzenesulfonate (NaDDBS) as a dispersant in D₂O.⁸ However, they used 2500 wt% of NaDDBS for purification. This excess amount of dispersant can be a problem in further application of purified NH because the excess dispersant is hardly removable from NHa and affects the property of NHa. Moreover, the authors claimed that D₂O was critical for the purification of NHa because the density of NHa was similar to H₂O. This result showed that the separation of NHa only by its density did not work well.

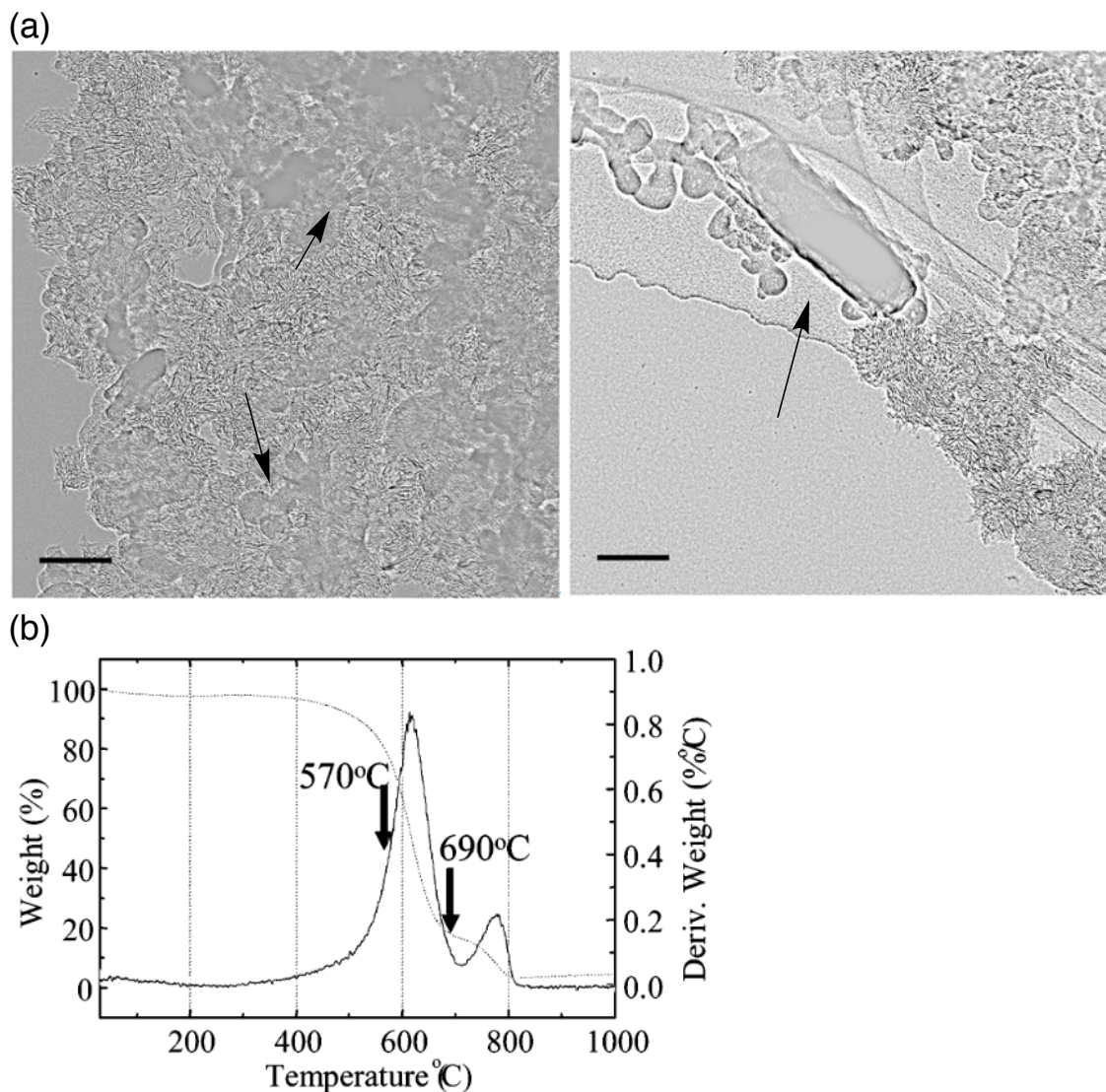


Figure 3-1. Characterization of GBs contained in NHa. (a) A representative TEM images of as-purchased NHa containing GBs (indicated by arrows.). Scale bar shows 100 nm. (b) Thermogravimetric analysis of NHa and GB burned around 600 °C and 800 °C, respectively. Adapted with permission with ref. 6. Copyright 2005 American Chemical Society.

3.1.2. Superhydrophobicity

The hydrophobicity of the material surfaces is determined not only by the chemical property of the surface but also by the surface roughness. It is well-known that a lotus leaf repels water droplets and keeps its dried state, which is called as a “lotus-effect” and superhydrophobicity. This phenomenon is achieved by its surface structure with densely aligned nano-sized hydrophobic materials. The surface roughness is critical

for a surface to be superhydrophobic (the contact angle of the surface is greater than 150°) as revealed by a series of experiments to mimic the structure of a lotus leaf.⁹

The origin of superhydrophobicity was first theoretically explained by Wenzel. Wenzel modified Young-Dupré equation¹⁰ (Figure 3-2a) of the contact angle by introducing a factor of roughness, r_s , which is the ratio of total surface area to the corresponding flat surface (Figure 3-2b).

$$\gamma_{SL} + \gamma_{LV} \cos \theta_Y = \gamma_{SV} \quad (1)$$

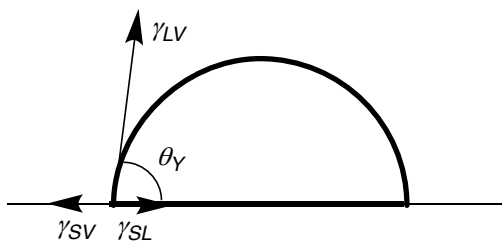
$$\cos \theta_W = r_s \cos \theta_Y \quad (2)$$

where γ_{SL} , γ_{LV} , γ_{SV} are interfacial surface tension between solid-liquid, liquid-vapor, and solid-vapor interface, and θ_Y , θ_W are actual and apparent contact angle. This Wenzel's equation was further extended by Cassie and Baxter.¹¹ In the surface with higher roughness, the liquid does not go into the pore in the structure and showed a larger contact angle than that expected from Wenzel's equation. In the Cassie-Baxter model, surface hydrophobicity is explained as a combination of an apex of surface roughness and vapor as shown in eq 3 (Figure 3-2c).

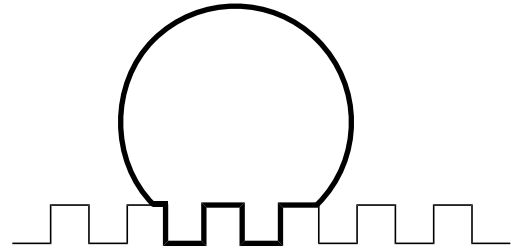
$$\cos \theta' = f_1 \cos \theta_Y - f_2 \quad (3)$$

where f_1 and f_2 were surface fraction of water and air, and θ' represents apparent contact angle. Considering the Cassie-Baxter model can be changed to the Wenzel model by adding force,¹² which suggested Cassie-Baxter state is a kind of kinetically trapped state, the tip selective functionalization efficiently reduce the kinetic barrier of superhydrophobicity of a rough surface.

(a) Young-Dupré equation



(b) Wenzel model



(c) Cassie-Baxter model

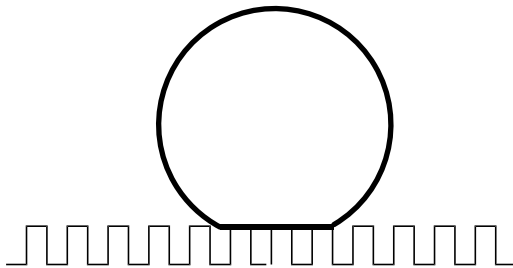


Figure 3-2. Schematic illustration of (a) Young-Dupré model, (b) Wenzel model, and (c) Cassie-baxter model.

3.1.3 Utilization of cyclodextrins as a shape-cognitive dispersant of NHa for purification of GB from mixture

From the insight into the relationship between hydrophobicity and roughness of a surface, I surveyed the tip-cognitive functionalization of NH aggregates via cavity and rim binding. Here, cyclodextrins (CDs) acted as a surfactant without conventional structure with a polar head and non-polar tail¹³ by mimicking hemimicelle structure of surfactant, and dispersed NHa efficiently and shape-selectively (Figure 3-3).

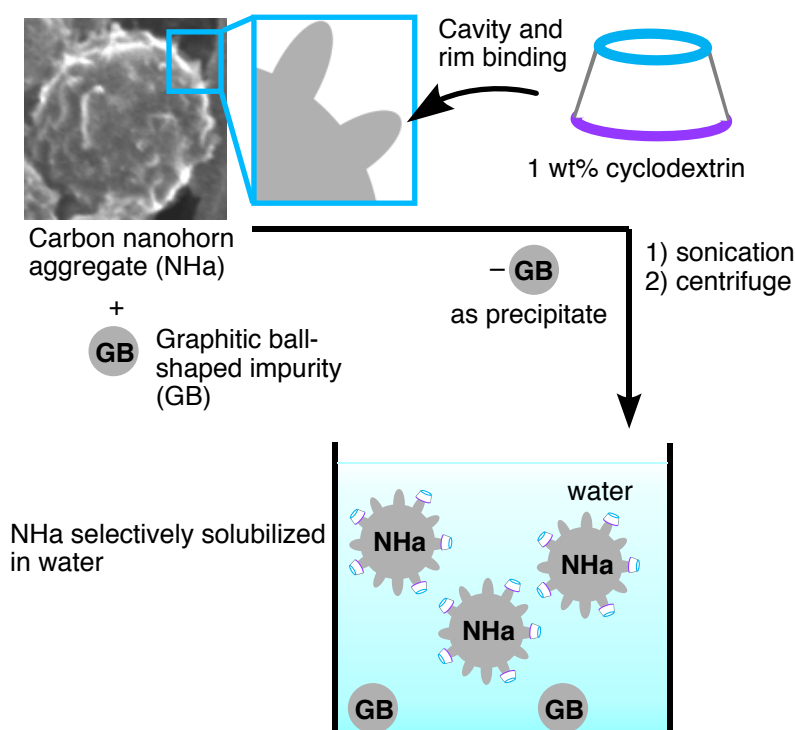


Figure 3-3. Schematic illustration of shape-cognitive binding of cyclodextrins to the tip of NHa for purification of NHa

3.2. Results and discussion

3.2.1 Dispersion of NHa with CDs

To confirm efficient solubilization of NHa in water and evaluate the effect of curvature-selective binding of CDs, I investigated the ability of saccharides to disperse NHa in water as shown in Figure 3-4a. 5.0 mg of NHa and 0.05 mg of saccharides (α -CD, β -CD, γ -CD, D-glucose, and amylose) were added to 10 mL of deoxygenated water. Then, the mixtures were sonicated for 5 min with vigorous stirring. The obtained

dispersions were heated at 70 °C and homogenized by brief sonication. β -CD required the heating process to form the stable dispersion reproducibly. The low dispersion ability of β -CD without heating was shown by dynamic light scattering (DLS) analysis of the dispersion before heating (Figure 3-4b). Thus, the dispersion of β -CD treated NHa (green) showed three peaks around 160, 460, 1280 nm, while the dispersion obtained using α - and γ -CD (blue and red, respectively) showed a single peak with a peak center around 140 nm (Figure 3-4c). The difference came from the adsorbed amount of CDs on the tip of NHs. At 25 °C, β -CD attached on only 1.0% of NHs. On the other hand, α - and γ -CD attached to 2.0 and 3.6% of NHs. The weak binding of β -CD is because internal hydrogen bonding at the wide rim, which was considered as the cause of low solubility of β -CD compared with α - and γ -CD¹⁴ prevented the interaction between secondary OH groups and NH surface. By heating at 70 °C, the hydrogen bonds were broken, and RB occurred efficiently as observed in the increase in the amount of binding to the tips (4.7% at 70 °C). Therefore, the NHs were well dispersed after heating in all CDs, and DLS analysis showed the single peak around 120 nm, which is well matched with the size of NHa (50–100 nm). Thus, I used the same condition for the evaluation of the ability of other saccharides to disperse NHa.

The NHa dispersed in the top half layer were filtered and isolated as a black powder in $22 \pm 2\%$, $23 \pm 6\%$, and $27 \pm 6\%$ yield for α -, β - and γ -CD, respectively (Figure 3-4d). On the other hand, the other saccharides failed to disperse NHa in this condition, and isolated yields were 4 ± 2 and $5 \pm 2\%$ for D-glucose and amylose, which were the same yield as a controlled experiment without any additives ($4 \pm 2\%$). Considering the binding of glucose to the activated carbon and that of amylose to the sidewall of multi-walled CNT were reported,^{15,16} the difference between CDs and non-cyclic saccharides were binding efficiency to the tip part of NHa and showed the importance of binding to the tips of NHs via CB and RB for efficient solubilization of NHa in water. Single-walled carbon nanotube (CoMocat®) nor graphite that lack spherical tips were not dispersed in water by CDs (Figure 3-5). The result showed the importance of shape-cognitive binding for efficient solubilization and the potential of CDs for separating carbon materials based on their shapes.

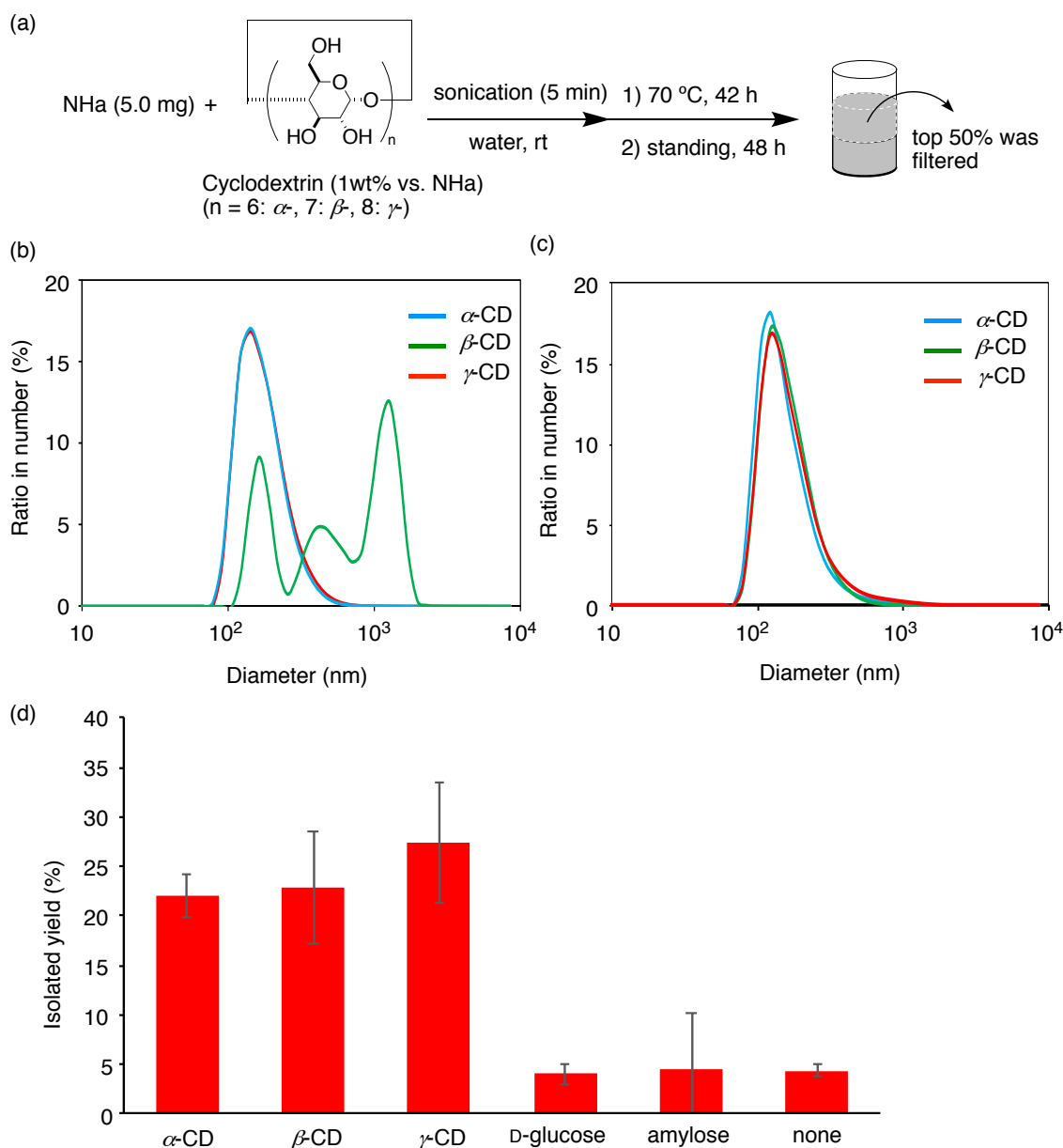


Figure 3-4. Dispersion and characterization of NHa with cyclodextrins. (a)

Preparation of dispersion of NHa with CDs.; (b) Dynamic light scattering data of size distribution of NHa dispersed by CDs after sonication for 5 min at room temperature.; (c) Dynamic light scattering data of size distribution of NHa dispersed by CDs after heating for 42 h at 70 °C.; (d) The isolated yield of NHa dispersed in top half layer of water after complexation with various saccharides.

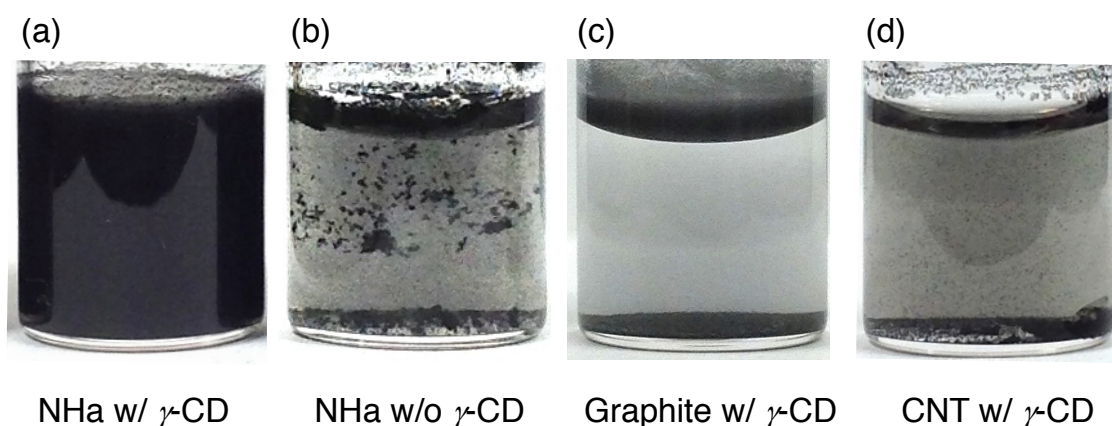


Figure 3-5. The pictures of carbon materials mixed and sonicated with 1 wt% of γ -CD. (a) NHa dispersed with γ -CD. (b) NHa sonicated in water without addition of γ -CD. (c) graphite mixed and sonicated with 1 wt% of γ -CD. (d) carbon nanotube mixed and sonicated with 1 wt% of γ -CD.

3.2.2 Analysis of dispersed NHa

The absence of GB in the dispersed NHa was examined by TG analyses under dry air and TEM observation. Figure 3-6a, b shows the TG curve and their derivatives of NHa in the dispersion with γ -CD (red), as-purchased NHa (black), and γ -CD (gray). The results showed that NHa dispersed by γ -CD was free of GB, whose combustion peak was appeared around 700–800 °C in the as-purchased NHa. Moreover, the γ -CD-treated NHa only contained the fraction burned before 680 °C, indicating the possibility of fractionation between NHa based on their shape. γ -CD was burned from 350 °C and not observed in dispersed NHa because only 1 wt% against NHa was used to disperse NHa.

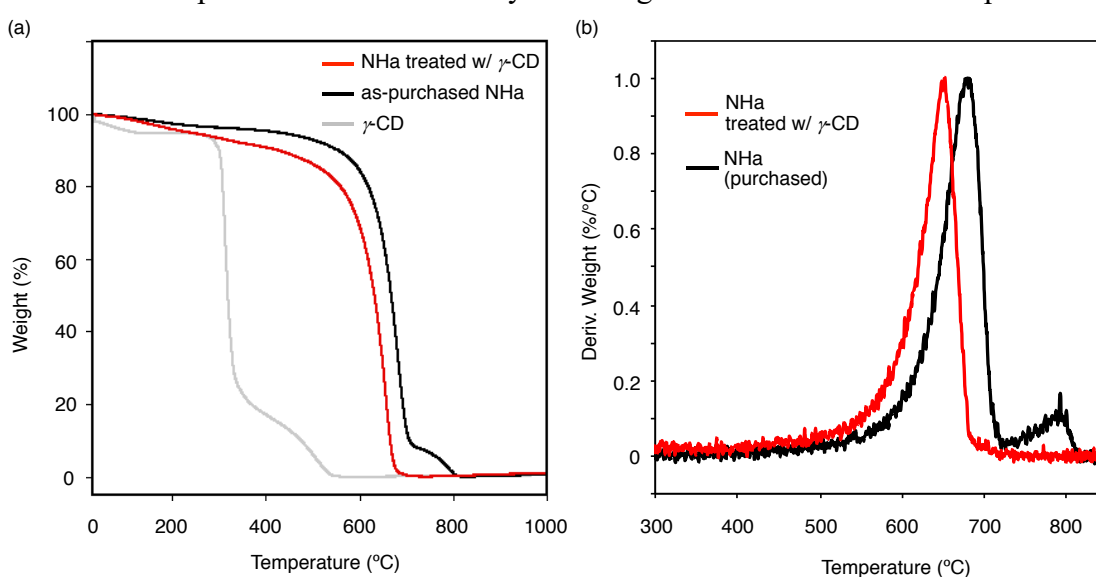


Figure 3-6. Thermogravimetric analysis of NHa dispersed by γ -CD. (a) Weight-

temperature curve of NHa treated with γ -CD (red), as-purchased NHa (black), and γ -CD (gray), (b) temperature differentiation of the weight curves of NHa treated with γ -CD (red) and as-purchased NHa (black)

TGA of NHa dispersed by α - and β -CD was also conducted and showed that α - and β -CD also achieved selective dispersion of NHa via only rim binding modes from the mixture with GBs (Figure 3-7a). These results showed that the purification of NHa could be achieved only by RB, and suggested the utility of RB for the recognition of materials larger than the cavity size of CDs. Interestingly, the combustion peaks of γ -CDs observed in the differential curve (Figure 3-7b, red) was 20 °C lower than α - and β -CD (blue and green, respectively), which suggested that three CDs preferentially solubilized slightly different NHa based on their binding selectivity to the apex of NHs.

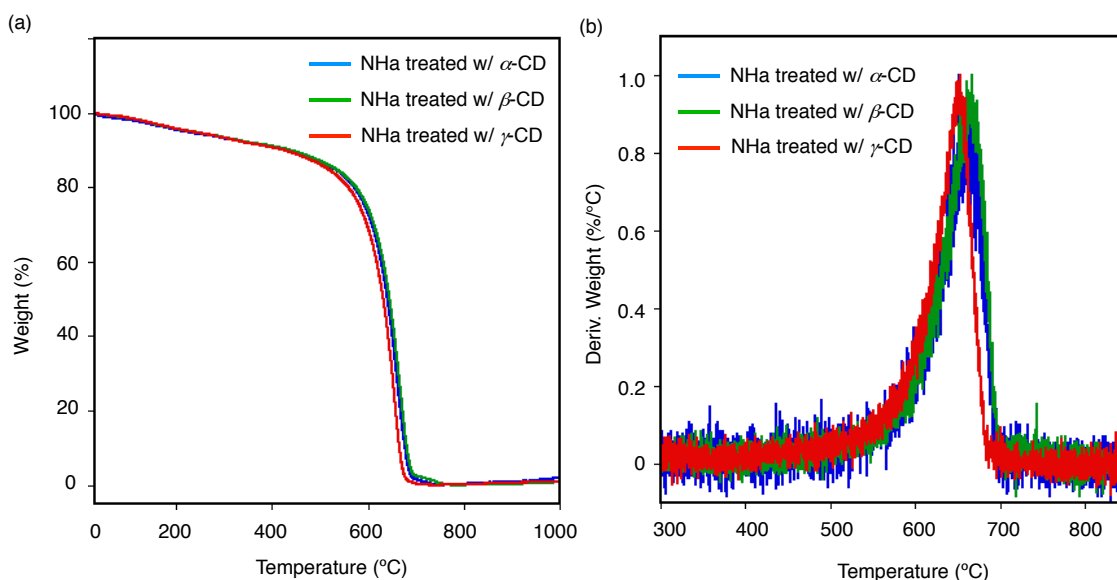


Figure 3-7. Thermogravimetric analysis of NHa dispersed by α -, β -, and γ -CD. (a) Weight-temperature curve of NHa treated with α -CD (blue), β -CD (green), and γ -CD (red), (b) temperature differentiation of the weight curves of NHa treated with γ -CD (red), β -CD (green), and γ -CD (red).

TEM observation confirmed the removal of GBs in γ -CD-treated NHa. In the representative images, horn-rich NHa and a small amount of horn-less NHa were observed, while the micrometer-sized particle was not observed (Figure 3-8). Importantly, the horn structures on the surface of NHa were clearly observed without covering by CD molecules because only 1 wt% of CDs were used.

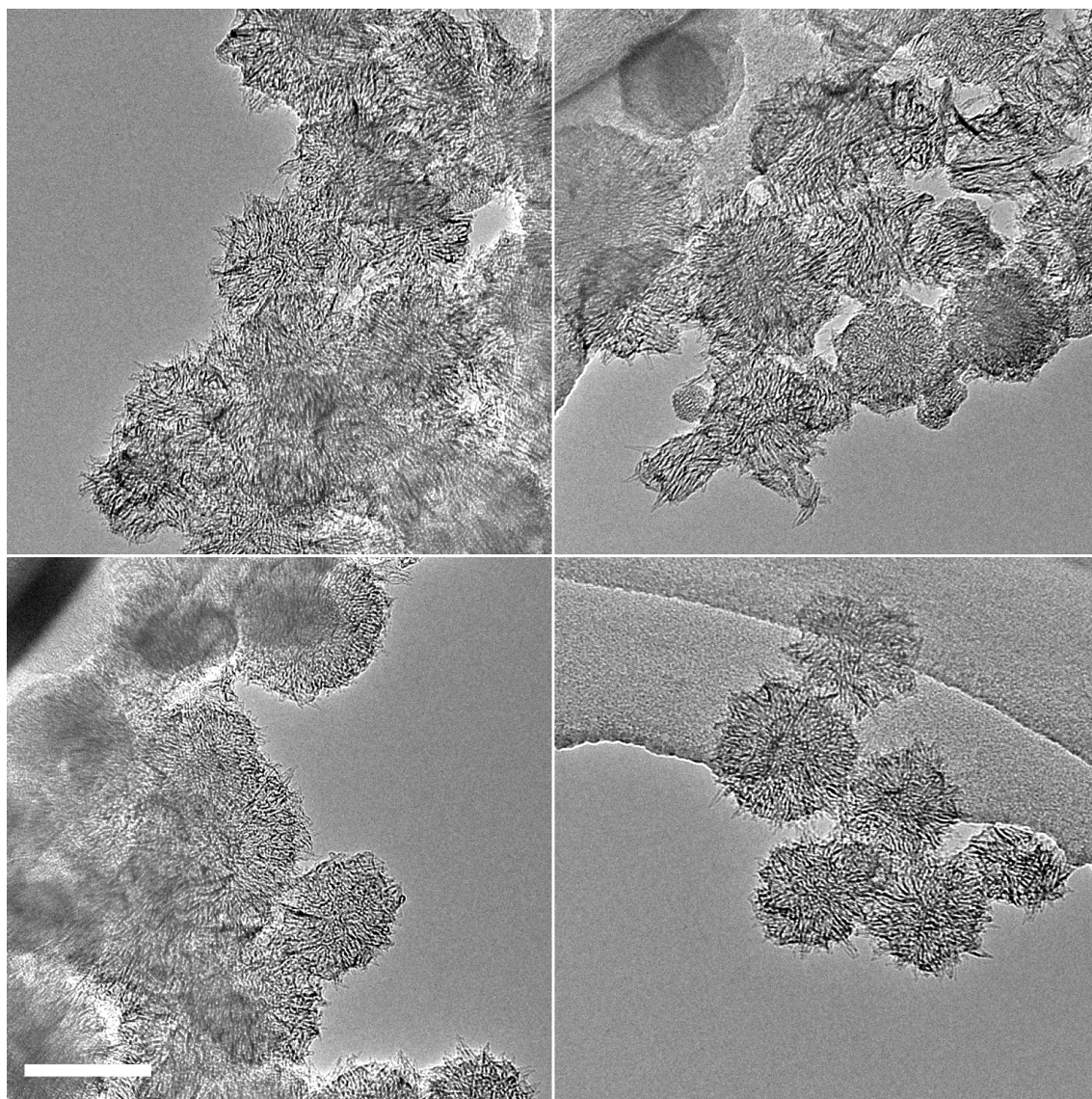


Figure 3-8. TEM images of GB-free NHa treated with γ -CD

3.2.3 Re-dispersion of CD/NHa in water

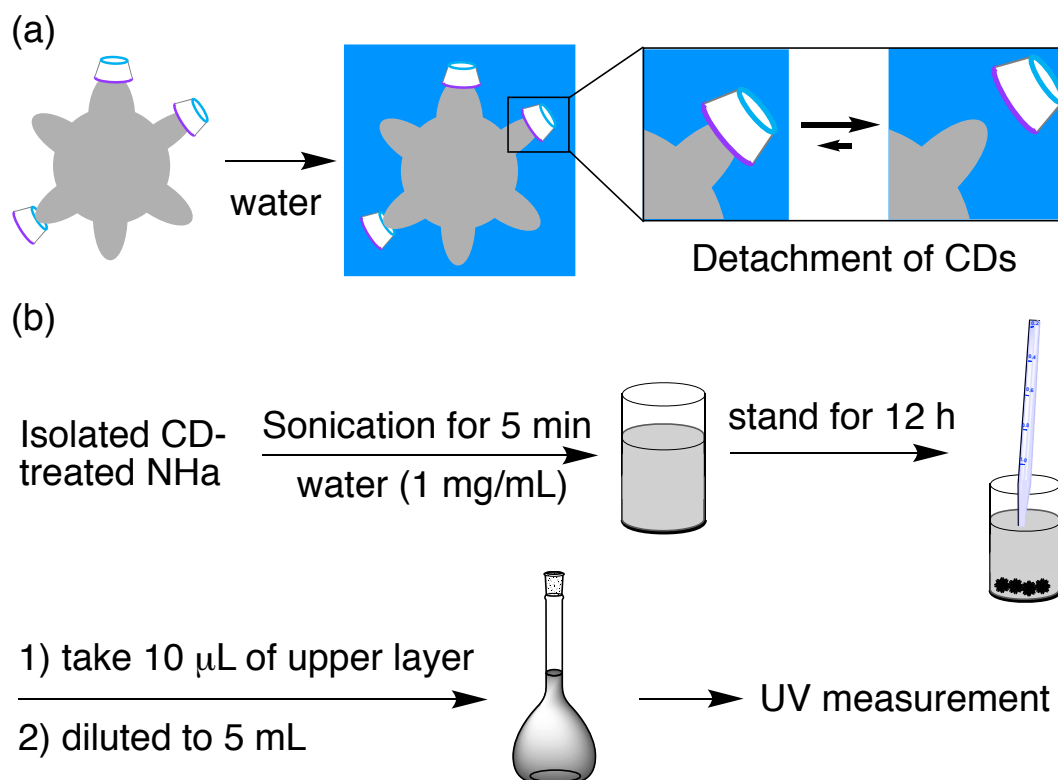
For the isolation of pure NHa, the removal of CDs is important. To investigate the removability of CDs from the surface of NHs by washing with water, CD-attached NHa were dispersed by CDs in pure water. No free CD was present in water at first, therefore the equilibrium shifted to desorption (Scheme 3-1a). I re-dispersed isolated CD-treated NHa (1.0 mg) in pure water (1 mL) by bath sonication for 5 min. For all CDs, NHa were dispersed in water and showed the stability of tip binding of CDs via CB or RB modes.

The re-dispersion of α - and β -CD was precipitated after standing for 12 h at room temperature as shown in Figure 3-9a. On the other hand, γ -CD kept dispersion after

12 h. The dispersed amount after 12 h were quantitatively investigated by UV-vis spectroscopy (Scheme 3-1b). The absorption at 260 nm, which was characteristic of tubular graphitic surface such as carbon nanotubes^{17,18}, revealed that $8 \pm 7\%$, $2 \pm 1\%$, and $31 \pm 12\%$ of NHa were still dispersed in water after 12 h by α -, β -, and γ -CD, respectively (Figure 3-9b). There were two possible reasons for the difference in the desorption of CDs. One possible reason is that CB of CD was kinetically stable than RB of CD, therefore CB of γ -CD remained in the desorption experiment. The other reason is that γ -CD bound to the wider size range of the tips of NHs than α - and β -CD, and the absolute amount of tip binding of CDs, which was considered to affect the dispersibility directly, was the largest in γ -CD. From these results, I concluded that α -CD was the best for the purification of NHa.

Scheme 3-1. Re-dispersion experiments of CD/NHa to evaluate removability of CDs.

(a) Schematic illustration of detachment of CDs in re-dispersion of CD/NHa, (b) Determination of dispersed amount of NHa in re-dispersion after standing for 12 h.



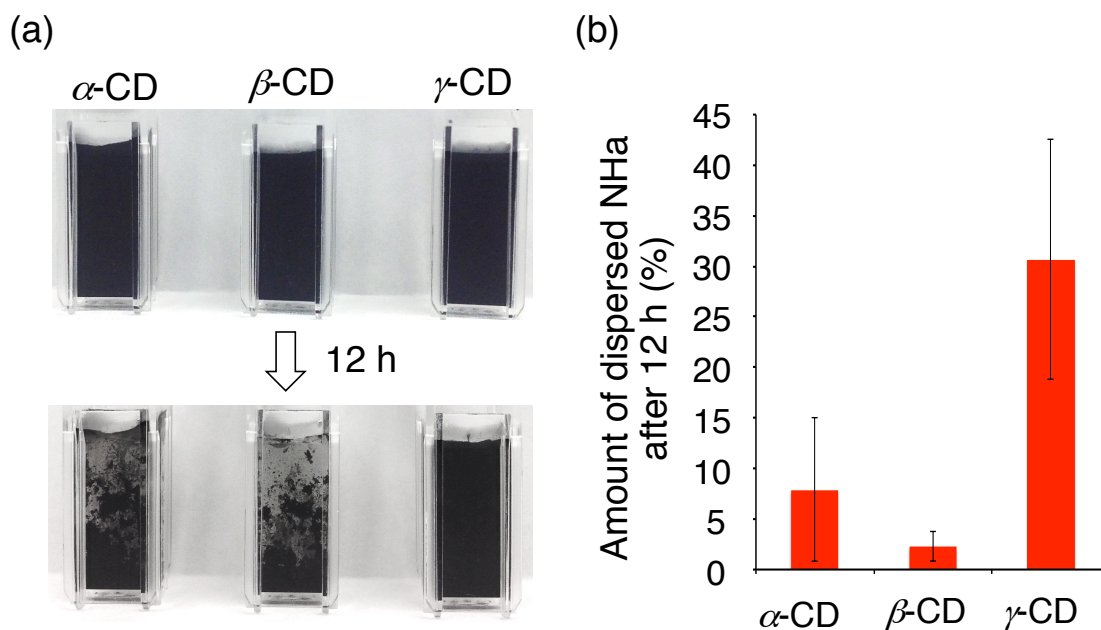


Fig. 3-9. Re-dispersion of CD/NHa. (a) pictures of re-dispersion of CD/NHa in water at 5 min and 12 h, (b) The amounts of NHa after re-dispersed for 12 h

3.2.4 A large-scale purification of NH aggregates by using α -CD

To establish a large-scale purification of NHa, I first optimized the purification method of NHa. In small-scale experiments, the separation of GB was conducted by standing after dispersion with CDs. However, the standing required a longer time as the scale become larger. For example, α -CD-treated NHa still contained 2wt% of GB after standing for 48 h, and the removal of GB was completed after 72 h (Figure 3-10). To accelerate the separation process, I utilized centrifugation for the system. Considering 72 h was necessary at 1 g to precipitate GBs by 4 cm, I set the relative centrifugal force as 1500 g to separate GB in 10 cm solution height within 10 min.

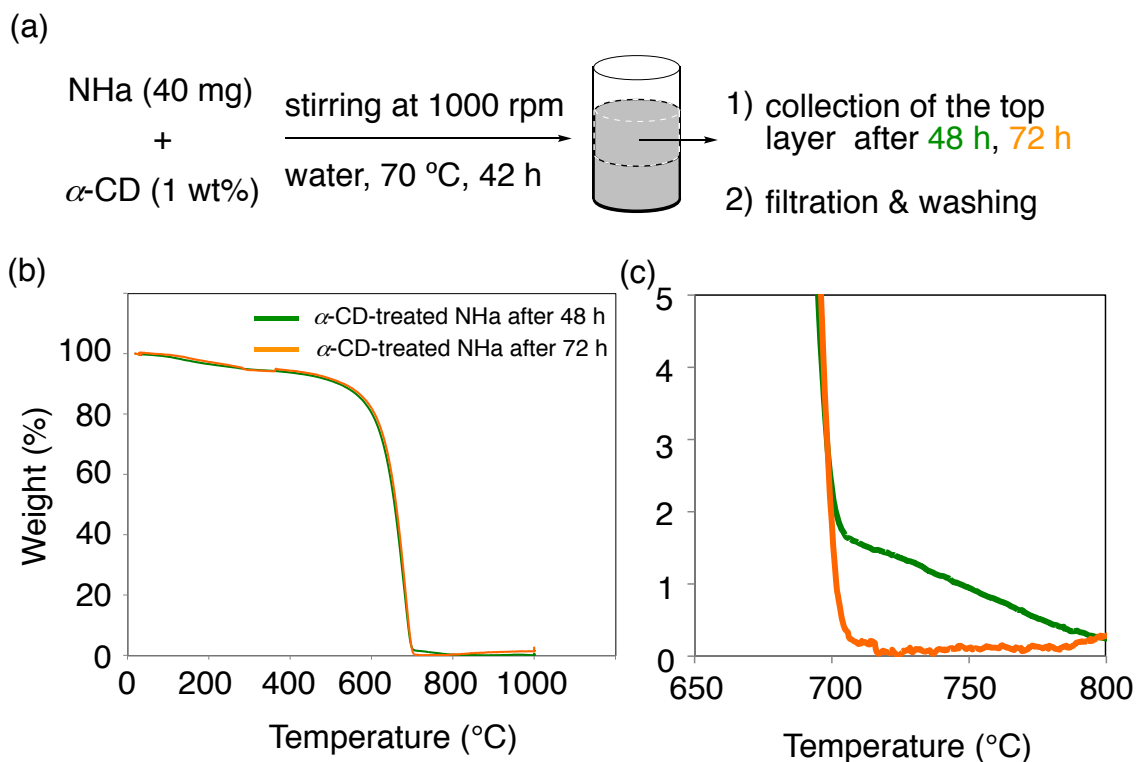


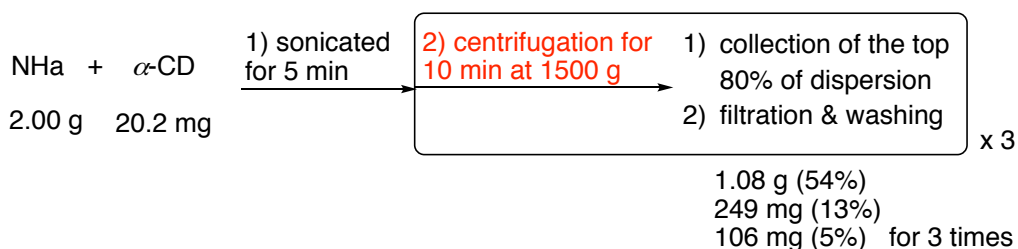
Figure 3-10. Purification of 40 mg of NHa and thermogravimetric characterization of purified NHa. (a) Solubilization and purification of 40 mg of NHa with α -CD by standing for 48 and 72 h, (b) Weight-temperature curve of CD/NHa in dispersion left for 48 h (green) and 72 h (orange), (c) Magnified figure of (b) between 650 °C to 800 °C corresponding to burning of GB.

Then, large-scale purification was conducted. NHa (2.00 g) and α -CD (20.2 mg) were mixed in water (800 mL) and sonicated for 5 min to obtain a black dispersion. The dispersion was centrifuged at 1500 g for 10 min, and the top 80% layer of the dispersion was filtrated through a membrane filter with a 200 nm pore size. The obtained solid was washed with water and ethanol (20 mL \times 3, respectively) to obtain 1.08 g of NHa (54% recovery) as a black powder after drying at 25 °C for 6 h. NHa were further collected by repeating the centrifugation and filtration two more times for the remained dispersion to obtain 249 mg (13%) and 106 mg (5%) of NHa, respectively (Scheme 3-2. TG analysis confirmed that the complete disappearance of GB in the first crop of purified NHa (Figure 3-11a). In the second and third crops, a small amount of GB remained, however, the amount was less than 0.5 wt% (Figure 3-11b,c).

Interestingly, the obtained TG of purified NHa was different from that of NHa purified by centrifugation of an ethanol dispersion.¹⁹ For comparison with NHa purified without CDs, NHa (20.0 mg) were dispersed in ethanol (8 mL) by bath-sonication for 15

min. The obtained dispersion was centrifuged at 667 or 167 g, and then the top 80% of the dispersion was taken and filtered to obtain 8.4 mg (42%) and 10.3 mg (51%) of NHa, respectively, after drying under vacuum. The TG curve of NHa purified in ethanol showed that enrichment of the fraction burned around 700 °C, and the ratio of the fraction increased with stronger centrifugation (Figure 3-11d). The result showed that the density of NHa including in the fraction was lowest in the as-purchased NHa. This tendency was clearly opposed to NHa purified by CDs, considering the purification with γ -CD in a small-scale shifted the peak of combustion to 20 °C lower temperature. The result suggested that the separation with CDs was not based merely on the density of dispersed materials.

Scheme 3-2. Purification of NHa in a gram-scale using α -CD.



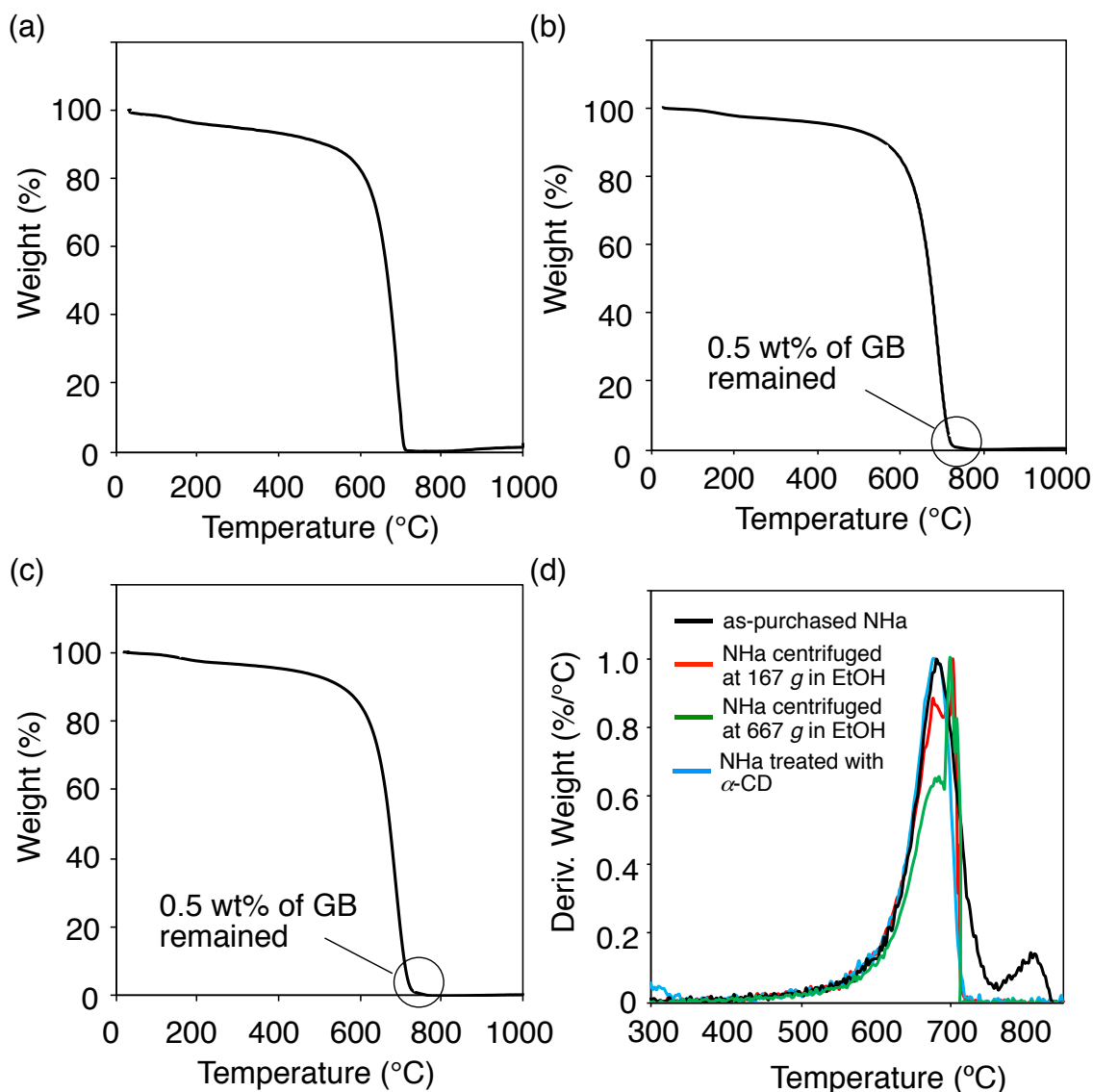


Figure 3-11. Thermogravimetric analyses of NHa purified in a gram-scale using α -CD. (a) Weight-temperature curve of purified NHa in the first collection, (b) Weight-temperature curve of purified NHa in the second collection, (c) Weight-temperature curve of purified NHa in the third collection, (d) Temperature differentiation of thermogravimetric curve of purified NHa dispersed and centrifuged in EtOH at 167 g (red) and 667 g (green), as-purchased NHa (black), and α -CD-treated NHa (blue).

3.2.5 Synthesis of GB-free amino-NHa

Amino-NHa has been synthesized by the reaction of NHa with NaNH_2 and utilized as a solid support to isolate a single molecule from bulk solution in the SMART-EM technique.²⁰ In the previous reports, amino-NHa was prepared from as-purchased NHa, which contained GB as an impurity. I anticipated the synthesis of GB-free amino-

NHa by using purified NHa.

First, I tried to synthesize amino-NHa by simply mixing NHa and NaNH₂ in liquid NH₃ following the previous report, however, the obtained product was poorly dispersed in water. The unsuccessful reaction was caused by tight aggregation of NHa, which was observed as an ill-dispersed reaction mixture during the amination reaction, because NHa was dried from water and hydrophobic interaction strengthened the aggregation. To solve this problem, I conducted grinding of NHa (200 mg) on a mortar for 5 min, and NHa was dried at 120 °C under vacuum for 6 h. The NHa was mixed with NaNH₂ (224 mg) in liq. NH₃ (320 mL) for 3 h at –33 °C. After removal of NH₃ at room temperature, the remaining solid was collected by filtration after dispersed in saturated NH₄Cl aqueous solution and washed with water to obtain 202 mg of amino-NHa as a black powder after dried under vacuum (Figure 3-12a). Thermogravimetric analysis showed that synthesized amino-NHa did not contain GB and the slight peak shifted to <660 °C due to amination reaction (Figure 3-12b). A dynamic light scattering of the water dispersion of the amino-NHa showed a good dispersibility observed as a single peak at 122 nm (Figure 3-12c).

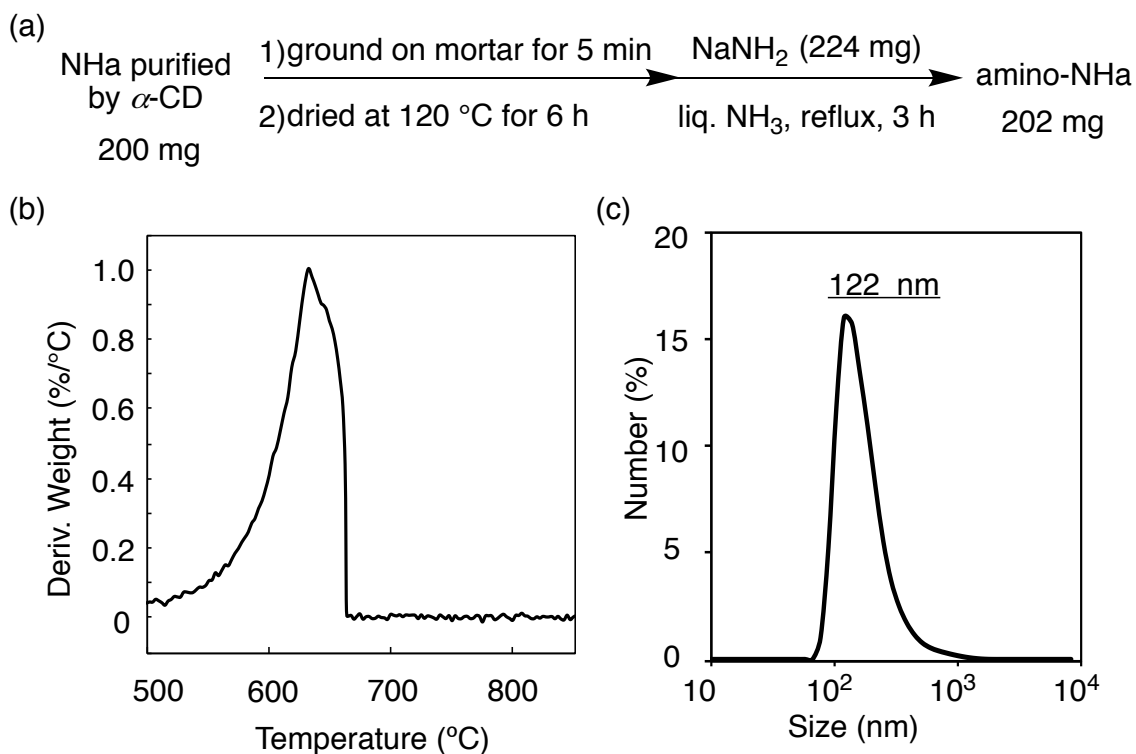


Figure 3-12. Synthesis and characterization of GB-free amino-NHa. (a) Amination of α -CD-treated NHa, (b) Temperature derivative of thermogravimetric curve of obtained amino-NHa, (c) Dynamic light scattering data of size distribution of amino-NHa dispersed in water

Size separation of amino-NHa by size-exclusion chromatography was also conducted to confirm the purity of NHa. Amino-NHa (0.1 mg) was dispersed in the 0.5 mL of water, and then passed through a column (sephacryl S-500, 15 cm, $\phi = 1.5$ cm, Figure 3-13a). Importantly, no solid remained at the top of the column because no GB remained. The dispersion was collected by 0.25 mL as shown in Figure 3-13c. Dynamic light scattering showed that the Z-average size of amino-NHa was separated from 299 nm in fraction 4 to 159 nm in fraction 9. Almost all of amino-NHa was recovered after passing the column (91%), and the remaining 9% was considered to be mainly trapped at the cotton as shown in Figure 3-13b.

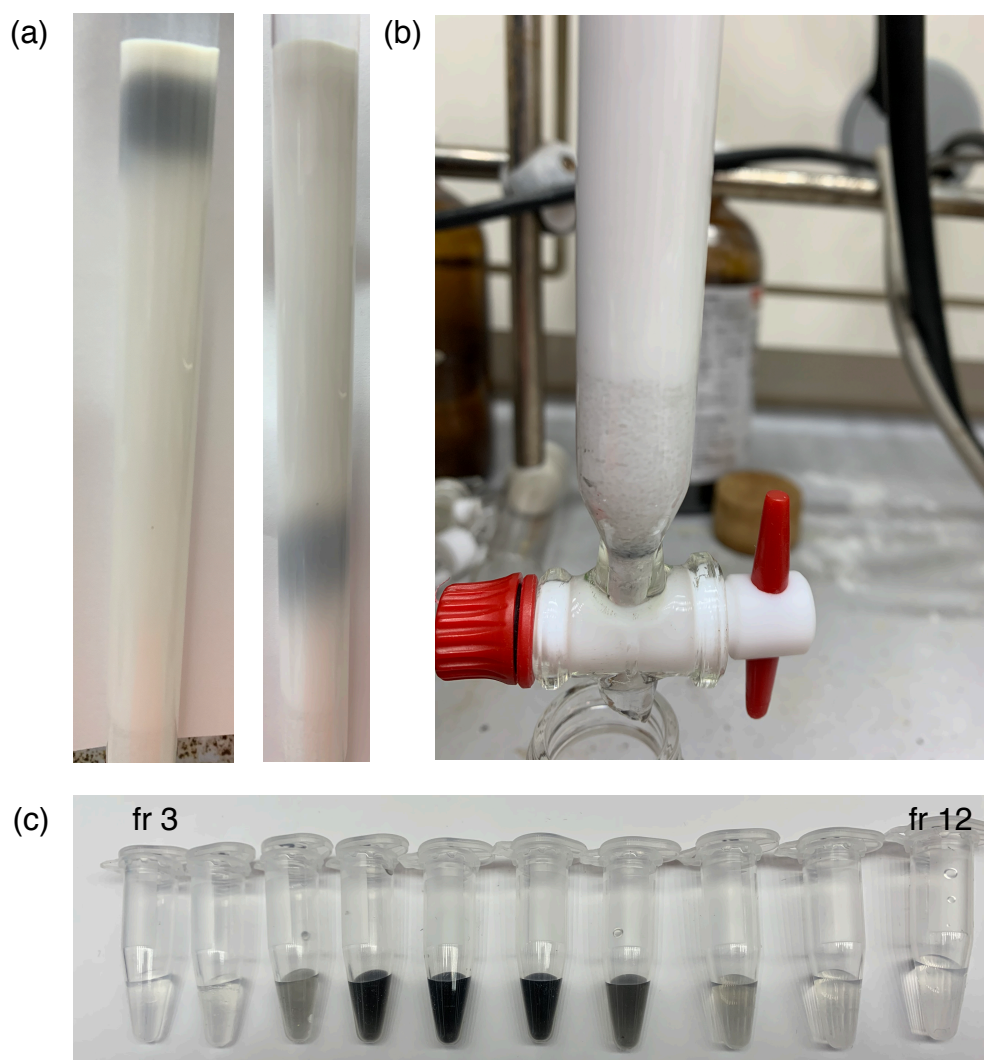


Figure 3-13. Separation of GB-free amino-NHa by size-exclusion chromatography. (a) Pictures of amino-NHa passing through size-exclusion chromatography. (b) Amino-NHa stacked at the cotton. (c) Fraction of separated amino-NHa.

3.3 Summary

In summary, I demonstrated solubilization and purification of NHa from GBs by using CDs. CDs bound to the apex of NHs via mainly rim binding and efficiently reduced the hydrophobicity of the spiked surface of NHa. Gram-scale purification was achieved with α -CD, which was easily removed from the surface of NHa, after centrifugation and washing. Finally, the amination of purified NHa gave GB-free amino-NHa.

3.4 Experimental section

3.4.1 Materials

Unless otherwise noted, materials were purchased from Tokyo Kasei Co., Aldrich Inc., and other commercial suppliers and used after appropriate purification before use. Carbon nanohorn was purchased from NEC Co. (Lot No. 181-3-2). Distilled water was further purified with Millipore Milli-Q. TEM grid precoated with a lacy microgrid (NS-C15, pore size 1.5–8 μm) was purchased from Okenshoji Co., Ltd.

3.4.2 General

Bath sonication for dispersion of NHs in water was carried out on a Honda Electronics WT-200-M instrument. UV/vis/near-IR absorption was measured on a Jasco V-670 spectrometer. High resolution TEM was performed on a JEOL ARM-200F at 293 K under reduced pressure of 1.0×10^{-5} Pa in the sample column. Detailed observation conditions and procedures are described below. Scanning electron microscopy was conducted using FEI Magellan 400L. Dynamic light scattering (DLS) study was carried out on a Malvern Zetasizer Nano ZS machine. Centrifugation experiments were conducted on TOMY LC-100. Thermogravimetric (TG) measurement was conducted on a Rigaku Thermo Plus machine.

3.4.3 Evaluation of dispersity of NHa via complexation with saccharides

NH aggregates (NHa, 5.0 mg, containing ca. 10 wt% graphitic ball-shaped impurity) was stirred in an aqueous solution (10 mL) of saccharides (α , β , γ -CD, D-glucose, and amylose; 1 wt% for NH) at 70 °C (heated in a sand bath) for 42 h. The mixtures were cooled down to rt, and then sonicated (6 W) for 5 min at the same position in the bath sonicator. The resulting dispersion was left to stand for 48 h to precipitate ill-dispersed particles and their aggregates. The top layer (5 mL) was collected and filtered by suction, and the residual solid was washed with water (10 mL) to remove saccharides that are not bound to NH. The collected NHa was dried overnight under vacuum (60 Pa) with P_2O_5 as a drying reagent to obtain NHa conjugated with saccharides.

3.4.4 Evaluation of the stability of CD/NHa complexes

The isolated CD/NHa complex (1.0 mg) was re-dispersed in 1.0 mL of water by sonication for 5 min and then left to stand for 12 h. 10 μL of supernatant was collected with a syringe, diluted with water to 5 mL in a measuring flask, and then subjected to UV/vis absorption measurement (cell path = 1 cm) (Figure 3-14a). We used absorption at 260 nm assignable to the plasmon absorption of tubular graphite²¹ for determination of

concentration (Figure 3-14b) according to the calibration curve for γ -CD/NHa (Figure 3-14c). The dispersed amount of NHa after standing 12 h was determined to be 8%, 2% and 30% for α -, β - and γ -CD/NHa, respectively.

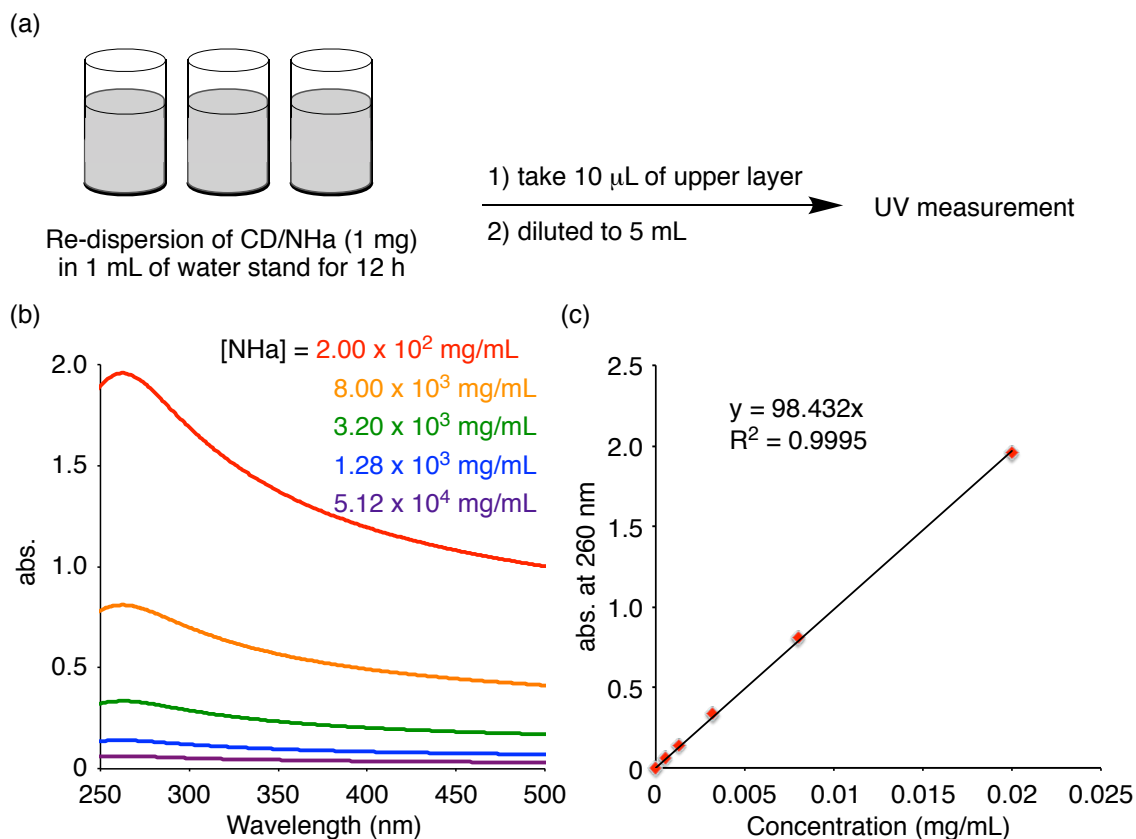


Figure 3-14. The evaluation of re-dispersion of CD/NHa complexes using UV-vis absorption. (a) Evaluation of dispersed amounts in re-dispersion of CD/NHa after 12 h, (b) UV-vis absorption of NHa of different concentration in water, (c) Calibration curve between the concentration of dispersed NHa and absorbance at 260 nm.

3.4.5 TG analysis

Before TG analysis, samples were dried up under vacuum (60 Pa) for at least 3 h at 120 °C. Weight loss of the NHa and CD/NHa complexes (ca. 2 mg) was measured from 30 °C to 1000 °C at the rate of 10 °C/min in dry air atmosphere with a flow rate of 100 mL/min using an alumina pan. Temperature derivatives of the weights curve were plotted from the weight loss curve.

3.4.6 Purification of NHa by complexation/decomplexation of α -CD

NHa (2.00 g) and 20.2 mg of α -CD was added into 800 mL of water in 1 L of

round-bottom flask. Then, the suspension was vigorously stirred for 30 min to immerse floating NH particles in water, and then bath-sonicated (6 W) for 5 min at 25 °C to obtain a black dispersion, which was transferred to centrifuge tubes in batch (50 mL \times 16, liquid height: 10 cm) and centrifuged at 1500 g for 5 min. From each tube, 40 mL of the top layer of each dispersion was collected by filtration through a PTFE membrane filter (pore size: 200 nm). The filter cake was washed successively with water (20 mL \times 3) and ethanol (20 mL \times 3). Note that the washing solvent and a filtered solid was mixed well with by using a pipette during filtration. The residue was dried under vacuum (60 Pa) at 25 °C for 6 h to obtain 1.08 g (54%) of NHa as black powder. Removal of GB impurity was confirmed by TG analysis (cf. Figure 3b).

Remaining NHa dispersion containing GB impurity (i.e bottom layer of each centrifugation tube) was collected together, sonicated for 1 min, and centrifuged again in batch (40 mL \times 4, liquid height: 8 cm) at 1500 g for 5 min. Top 32 mL of of the top layer of each dispersion was collected by filtration. After washing with water and ethanol (20 mL \times 3) and vacuum drying at 25 °C for 6 h, 249 mg of NHa (12%, containing 0.5 wt% GB impurity) was obtained as black powder.

The remaining dispersion was diluted to 50 mL with 2.5% α -CD solution and centrifuged at 1500 g for 5 min. Top 40 mL was collected by filtration, and washed with water and ethanol (20 mL \times 3). NHa (106 mg, 5.3%, containing 0.5 wt% GB impurity) was obtained as black powder after vacuum drying at 25 °C for 6 h.

3.4.7 Purification of NHa by centrifugation of EtOH dispersion

In a round-bottom flask, NHa (20.4 mg) was added to 8 mL of ethanol and sonicated for 15 min (6 W, bath sonicator) to form dispersion. After centrifugation in 15 mL centrifuge tubes (liquid height: 6 cm) at 1000 g for 6 min, top 6.5 mL of the dispersion was filtered through a PTFE membrane filter (ADVANTEC, pore size: 20 nm) and dried under vacuum at 25 °C for 12 h. 8.4 mg (43%) of GB-free NHa was obtained as black powder.

3.4.8 Preparation of amino-NHa from purified NHa

Purified NHa (200 mg) was gently ground in an agate mortar for 5 min and added into a 1 L of three-necked flask equipped with a dry-ice condenser. Liquid NH₃ (320 mL) was introduced from a gas NH₃ cylinder into the flask in a cooling bath (−78 °C) over 1.5 h, and the NHa was suspended by stirring. To the suspension, sodium amide (224 mg) was added, and the solution was refluxed for 3 h after removing the cooling bath. After removal of the solvent at room temperature by spontaneous evaporation in a ventilated

Chapter 3

hood, the residue was suspended in saturated NH_4Cl aqueous solution (100 mL) and filtered. The filter cake was washed with water ($50 \text{ mL} \times 3$) to obtain 202 mg of amino-NHa as black powder after drying at 25°C for 6 h.

3.5. References

- 1 Iijima, S.; Yudasaka, M.; Yamada, R.; Bandow, S.; Suenaga, K.; Kokai, F.; Takahashi, K. *Chem. Phys. Lett.* **1999**, *309*, 165–170.
- 2 Krungleviciute, V.; Migine, A. D.; Yudasaka, M. and Iijima, S. *J. Phys. Chem. C* **2012**, *116*, 306–310.
- 3 Ajima, K.; Yudasaka, M.; Murakami, T.; Maigné, A.; Shiba, K. and Iijima, S. *Mol. Pharm.* **2005**, *2*, 475–480.
- 4 Chechetka, S. A.; Pichon, B.; Zhang, M.; Yudasaka, M.; Bégin-Colin, S. Bianco, A. and Miyako, E. *Chem. Asian. J.* **2015**, *10*, 160–165.
- 5 Miyawaki, M.; Yudasaka, M.; Azami, T.; Kubo, Y. and Iijima, S. *ACS Nano* **2008**, *2*, 213–226.
- 6 Fan, J.; Yudasaka, M.; Kasuya, D.; Azami, T.; Yuge, R.; Imai, H.; Kubo, Y. and Iijima, S. *J. Phys. Chem. B* **2005**, *109*, 10756–10759.
- 7 Bandow, S.; Kokai, F.; Takahashi, K.; Yudasaka, M.; Qin, L. C. and Iijima, S. *Chem. Phys. Lett.* **2000**, *321*, 514–519.
- 8 Zhang, M.; Yudasaka, M.; Miyawaki, J.; Fan, J. and Iijima, S. *J. Phys. Chem. B* **2005**, *109*, 22201–22204.
- 9 Latthe, S. S.; Terashima, C.; Nakata, K.; Fujishima, A. *Molecules* **2014**, *19*, 4256–4283.
- 10 Young, T. *Philos. Trans. R. Soc. Lond.*, **1805**, *95*, 65–87.
- 11 Cassie, A. B. D.; Baxter, S. *Trans. Faraday Soc.* **1944**, *40*, 546–551.
- 12 Lafuma, A. and Quéré, D. *Nat. Mater.* **2003**, *2*, 457–460.
- 13 J. N. Israelachvili, *Intermolecular and Surface Forces* 3rd ed., Elsevier: Burlington, MA, **2011**.
- 14 Jozwiakowski, M.; Connors, K. A. *Carbohydr. Res.* **1985**, *143*, 51–59.
- 15 Dornath, P. Ruzycky, S. Pang, S. He, L. Dauenhauer, P. and Fan, W. *Green Chem.* **2016**, *18*, 6637–6647.
- 16 Star, A. Steuerman, D. W. Heath, J. R., Stoddart, J. F. *Angew. Chem. Int. Ed.* **2002**, *41*, 2508–2512.
- 17 Huang, X.; Mclean, R. S.; and Zheng M. *Anal. Chem.* **2005**, *77*, 6225–6228.
- 18 Kramberger, C.; Hambach, R.; Giorgetti, C.; Rummeli, M. H.; Knupfer, M.; Fink, J.; Büchner, B.; Reining, L.; Einarsson, E.; Maruyama, S.; Sottile, F.; Hannewald, K.; Olevano, V.; Marinopoulos, A. G.; and Pichler, T. *PRL*, **2008**, *100*, 196803.
- 19 T. Yamaguchi, S. Bandow, S. Iijima, *Tanso*, **2008**, *232*, 72–76.
- 20 E. Nakamura, *Acc. Chem. Res.*, **2017**, *50*, 1281–1292.
- 21 H. Isobe, T. Tanaka, R. Maeda, E. Noiri, N. Solin, M. Yudasaka, S. Iijima, E. Nakamura, *Angew. Chem. Int. Ed.* **2006**, *45*, 6676–6680.

Chapter 4.

Summary and Perspective

Chapter 4

Chapter 4

In the present thesis, a new binding mode of CDs other than cavity inclusion was discovered by utilizing TEM observation, and it was applied to solubilize hydrophobic material. Microscopic analysis has an advantage in the analysis of mixture compared with spectroscopic analyses, which only give averaged information of mixture. Its application to the detection of minor species in equilibrium revealed the rim binding complex of CDs. The rim binding mode contributed to the CD binding similarly to cavity binding and successfully solubilized nanocarbon in water.

第二章に関する記述については、5年以内に雑誌等で刊行予定のため非公開.

In Chapter 3, I demonstrated solubilization and purification of NH aggregates using CDs. NH aggregates contain horn-less impurity, which is co-generated in the production of NH aggregates. All CDs efficiently dispersed NH aggregates in water by binding to the apex of NHs, while glucose and amylose as a linear analog of CDs did not disperse NH aggregates well. Solubilization with α - and β -CD showed that cavity binding was not necessary for their action. Furthermore, binding to the apex of NHs achieved purification of NH aggregates by leaving GBs precipitated in water. The investigation of desorption of CDs from NH aggregates revealed that α - and β -CD detached faster than γ -CD. Therefore, α -CD was utilized for large-scale purification of NH aggregates by centrifugation of water dispersion and purified 2.00 g of NH aggregates in moderate yield. Non-selective purification by centrifugation of EtOH dispersion showed a different fraction of NH aggregates were separated and suggested that purification with CDs were based on the shape-recognition and not solely on the density of materials. Finally, purified NH aggregates were successfully utilized in further functionalization.

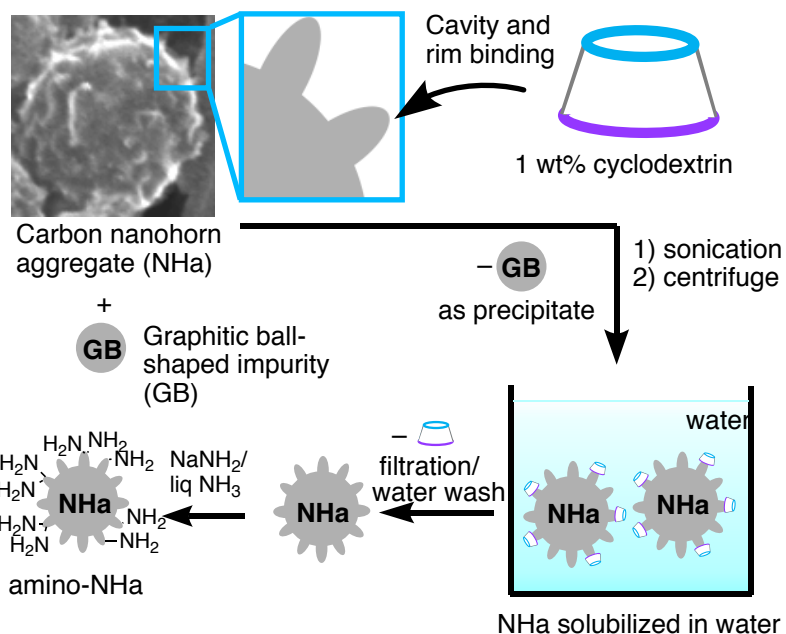


Figure 4-3. Solubilization and purification of NHa by binding of CDs to the apex of NHs via cavity and rim binding followed by centrifugation and amination.

The application of electron microscopic analysis to an equilibrium system enables us to investigate structure and differentiate each species present in the equilibrium. This is in clear contrast to conventional spectroscopic analysis, which only gives averaged information of the whole equilibrium. In the present study, we have demonstrated that a combination of SMART-EM and the NH library provides a tool not only to isolate the equilibrating species from solution for structure characterization but also to determine the thermodynamics governing the equilibria. We anticipate the application of this tool for thermodynamic and kinetic studies of various chemical events.

